

Article

# High-Resolution Magic Angle Spinning (HR-MAS) NMR-Based Fingerprints Determination in the Medicinal Plant *Berberis laurina*

Sher Ali <sup>1,\*</sup> , Gul Badshah <sup>1</sup>, Caroline Da Ros Montes D'Oca <sup>1</sup>, Francinete Ramos Campos <sup>2</sup>, Noemi Nagata <sup>1</sup>, Ajmir Khan <sup>3,4</sup> , Maria de Fátima Costa Santos <sup>1</sup> and Andersson Barison <sup>1,\*</sup> 

<sup>1</sup> NMR Lab, Department of Chemistry, Federal University of Paraná, Curitiba 81530-900, PR, Brazil; gulbadshahum1188@gmail.com (G.B.); caroline.ros@hotmail.com (C.D.R.M.D.); nnagata@ufpr.br (N.N.); fatima.mcs2529@gmail.com (M.d.F.C.S.)

<sup>2</sup> Department of Pharmacy, Federal University of Paraná, Curitiba 80210-170, PR, Brazil; francampos@ufpr.br

<sup>3</sup> School of Packaging, Michigan State University, East Lansing, MI 48824-1223, USA; ajmirkhan33@yahoo.com

<sup>4</sup> Institute of Chemistry, University of São Paulo, São Paulo 05508-000, SP, Brazil

\* Correspondence: alisherufpr@gmail.com (S.A.); anderbarison@gmail.com (A.B.)

Received: 11 April 2020; Accepted: 17 June 2020; Published: 11 August 2020



**Abstract:** *Berberis laurina* (Berberidaceae) is a well-known medicinal plant used in traditional medicine since ancient times; however, it is scarcely studied to a large-scale fingerprint. This work presents a broad-range fingerprints determination through high-resolution magical angle spinning (HR-MAS) nuclear magnetic resonance (NMR) spectroscopy, a well-established flexible analytical method and one of most powerful “omics” platforms. It had been intended to describe a large range of chemical compositions in all plant parts. Beyond that, HR-MAS NMR allowed the direct investigation of botanical material (leaves, stems, and roots) in their natural, unaltered states, preventing molecular changes. The study revealed 17 metabolites, including caffeic acid, and berberine, a remarkable alkaloid from the genus *Berberis* L. The metabolic pattern changes of the leaves in the course of time were found to be seasonally dependent, probably due to the variability of seasonal and environmental trends. This metabolites overview is of great importance in understanding plant (bio)chemistry and mediating plant survival and is influenceable by interacting environmental means. Moreover, the study will be helpful in medicinal purposes, health sciences, crop evaluations, and genetic and biotechnological research.

**Keywords:** *Berberis laurina*; metabolomic analysis; HR-MAS NMR; metabolites; chemometric analysis

## 1. Introduction

The family Berberidaceae consists of about 13 genera and 600 species, including the commonly known genus *Berberis* L., which is considered the main contributor with 500 species, including the species *Berberis laurina* Billb. [1]. The usual physiognomies nature of such genus are their highly spiny, deciduous shrubs or small woody trees with characteristic yellow flowers. This genus is well-known as a pharmacological source in traditional medicine systems since ancient times [1]. The species *B. laurina* Billb. (Figure 1) is frequently distributed in the Northern hemisphere, some Asian countries [1], and in some South American countries, particularly in the south and southeast of Brazil, as well as in Argentina, Uruguay, and Paraguay, where it is known as *Espinho-de-São-João*, *Berbéris-da-terra*, *Quina-cruzeiro*, *Uva-de-espinho*, *Espina-amarilla*, and *Palo-amarillo* [2]. Although there are a few missing statements of the complete chemical profiles related to *B. laurina* Billb., since, this gap has been correspondingly completed in the current work focused on the aerial (leaves and stems) and underground (roots) parts of the species.

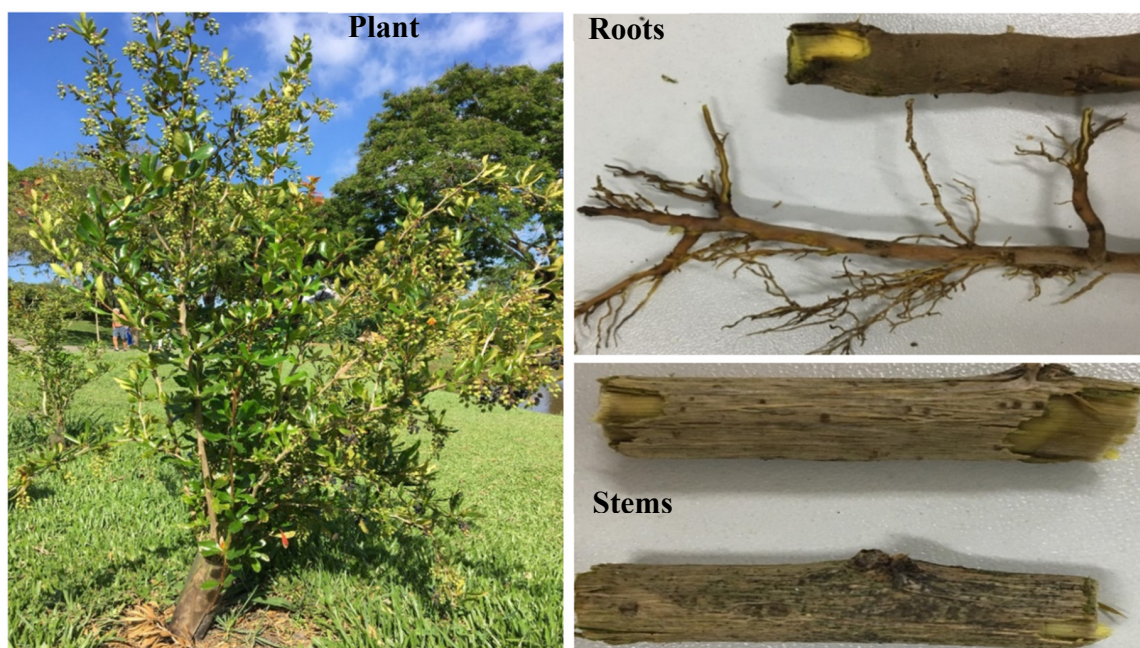


**Figure 1.** A representative specimen of *Berberis laurina* Billb. and its parts. The photos are available at [http://www.ufrgs.br/fitoecologia/florars/open\\_sp.php?img=11160](http://www.ufrgs.br/fitoecologia/florars/open_sp.php?img=11160).

Nuclear magnetic resonance (NMR) is worldwide well-established spectroscopic technique that allows to obtain information related to the genotype, phenotype, and intra- and interorganism classifications based on its origin and biological importance, environmental toxicity, and pollution [3–10]. In such, NMR spectroscopy is widely used in multidisciplinary “omics”, such as metabolomics, metabolic profiling, fingerprinting, and phenotyping [11–14], as well as in identification and structural determination of organic compounds in various samples such as food [4], ice [8], serum [10], environmental [15], material science [16], and water [17]. In addition, high-resolution magic angle spinning (HR-MAS) is a multipurpose NMR tool allowing the acquisition of NMR data directly from semi-solid (i.e., gel-like) materials (e.g., plant tissues) in their natural, unaltered states, without laborious sample preparation steps, and then preventing changes in the chemical composition during these process [18,19]. Moreover, the HR-MAS NMR technique uses specialized HR-MAS probes that allow to collect high-resolution spectra from heterogeneous samples with remarkably similar spectral resolutions as those observed for homogeneous samples in a liquid state (i.e., solution state).

Due to restricted and low molecular tumbling conditions, botanical samples contain several anisotropic trends such as dipolar (through bonds and space) interactions, magnetic susceptibility, and chemical shift anisotropy [18,20]. These trends directly affect T2 relaxation, which produces a nonuniform shift (line-broadening), also causing low signal-to-noise and resolution in NMR spectra [18,21–23]. Dipolar coupling is proportional to the “ $3\cos^2\theta - 1$ ” term in the second-order Legendre polynomial equation: “ $P_2(\cos^2\theta) = \frac{1}{2}(3\cos^2\theta - 1)$ ”. Therefore, the line-broadening effects coming from dipolar interactions can be minimized by spinning the sample at high spinning rates at the so-called magic angle ( $\theta_{MAS} = 54.74^\circ$ ) [18,22]. Additionally, in order to improve spectral resolution [18], the HR-MAS technique is to be applied to the swollen sample in a suitable NMR solvent that provides some molecular motions [19,22]. In addition to the liquid state, HR-MAS NMR has been used in metabolic analyses in human, plant, and food stuff quality managements, genotype, phenotype, and organism cataloging, with interindividual comparisons, environmental toxicity, and pollution [24–30]. Moreover, crowded spectral overlaps and chemical structure elucidations can be facilitated by mapping all homo- and heteronuclear correlations through multidimensional (nD) NMR approaches [31].

The plants (bio)chemically produce a composite assembly of different features of multiclass, small, organic metabolites as basic needs of energy, protections, and growth [29,32,33]. These molecular assemblies, even though normal growths, are highly affected through irregular environmental conditions. To trace such relationships (plant environments), since periodic investigations of metabolites are useful tools and, also, helpful in understanding the (bio)chemistry and other biological events [34]. Plants can adapt to any (un)suitable environments by rearranging their genetics to molecular outlines and productions to respond to unfeasible environmental impacts [35]. Additionally, this could provide excellent glimpses into chemical and biological research about vital relationships and to the discovery of new chemical entities with potential applications in medicinal chemistry [29]. Excepting metabolic mechanisms, interactive environmental effects to the molecular patterns within plant topology has been limited. In this regard, within plants, the topological order was measured through HR-MAS NMR-based fingerprinting, which was followed by multivariate statistical analysis such as principal component analysis (PCA) approach [11,12]. Since the study was sustained along seven months (October 2018 to April 2019) to spectroscopically and statistically correlate chemical alterations within aerial parts of the individuals in the associated period.

## 2. Results and Discussion

In present work, leaves, roots, and stems of *Berberis laurina* Billb. (Berberidaceae) were directly investigated in their natural state through  $^1\text{H}$  High-Resolution Magic Angle Spinning Nuclear Magnetic Resonance (HR-MAS NMR) approach, without sample pretreatment steps, and then preventing changes in the chemical compositions during extraction and isolation procedures. Following that, as the  $^1\text{H}$  NMR spectra taken in solution were remarkably like to those in semi-solid taken by means of HR-MAS (Figure S1), the liquid-state 2D NMR experiments were performed to facilitate metabolite identifications. In turn, a range of 17 primary and secondary specialized metabolites in all plant parts (leaves, stems, and roots) were detected (Figure 2).

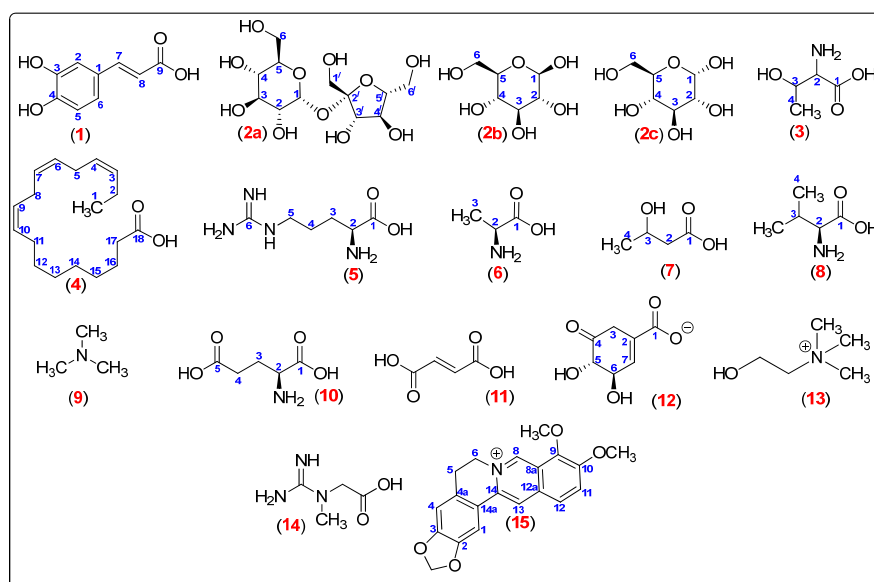


**Figure 2.** Metabolites identified in the leaves, stems, and roots of *Berberis laurina* (Berberidaceae).

The principal chemical constituents found in the leaves in comparison to stems and roots were caffeic acid (1), sucrose (2a),  $\beta$ -glucose (2b),  $\alpha$ -glucose (2c), threonine (3), fatty acids (Linolenic acid and 4), arginine (5), alanine (6), 3-hydroxybutyric acid (7), valine (8), trimethylamine (9), glutamic acid (10), fumaric acid (11), dihydroxy shikimate (12), choline (13), creatine (14), and berberine (15), as shown in Figure 2. In general, fairly to leaves, the stems but, remarkably, the roots were observed rich sources of berberine (15) (Figure S2).

### 2.1. $^1\text{H}$ HR-MAS NMR-Based Chemical Composition of the Leaves of *Berberis laurina*

The spectral profile acquired directly from the leaves of *B. laurina* (Figure 3) seemed to be very overlapped and difficult to clearly identify the signals from the chemical compounds. Thus, it was divided into three major segments: the high (aromatic; Figure 4, middle (carbohydrate; Figure 5), and low-frequency region (aliphatic region; Figure 6), which are discussed individually as follows.

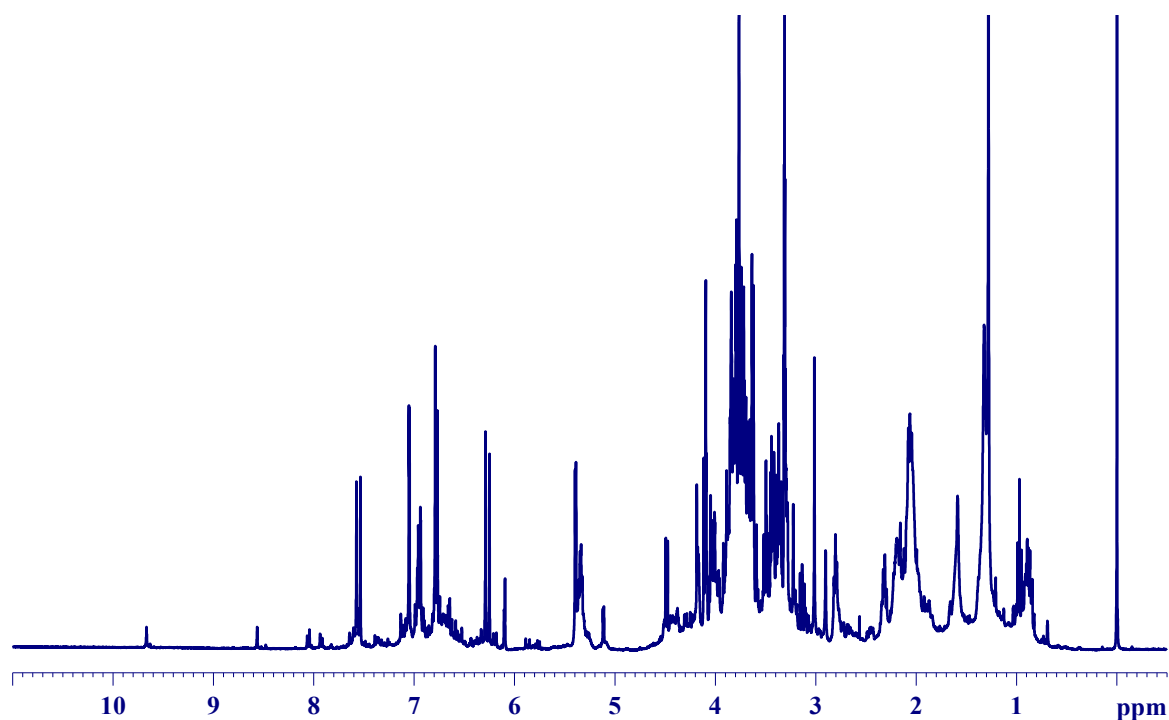


**Figure 3.**  $^1\text{H}$  HR-MAS NMR ( $\delta$   $-0.50$ – $11.00$ ) spectrum from the leaves of *Berberis laurina* (400 MHz,  $\sim 10$  mg swollen in  $40\text{-}\mu\text{L}$   $\text{CD}_3\text{OD}$ ).

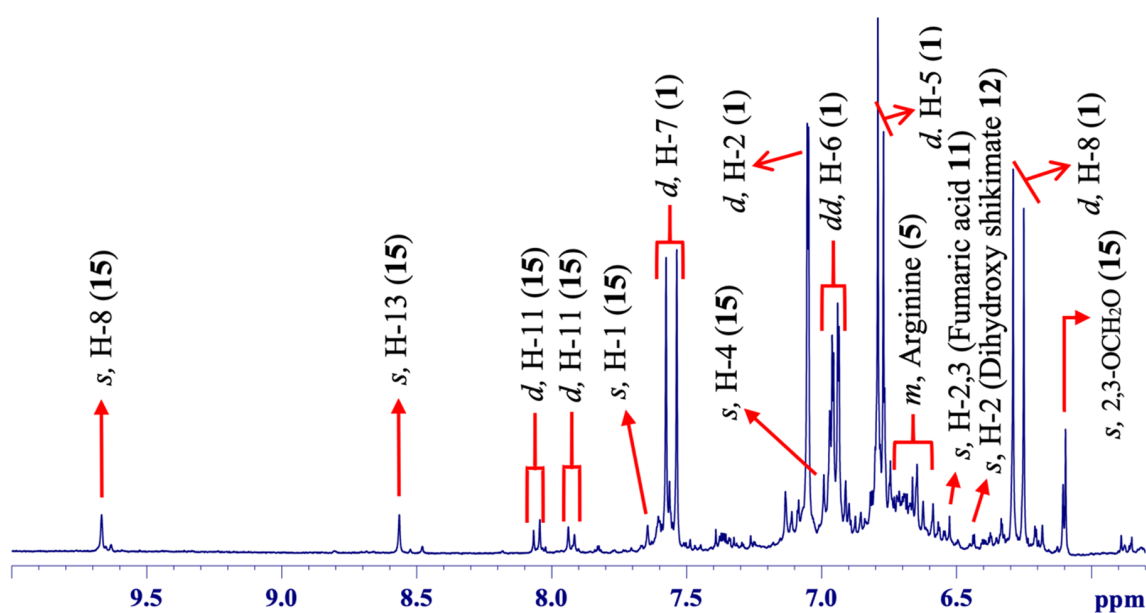


**Figure 4.**  $^1\text{H}$  HR-MAS NMR ( $\delta$   $5.80$ – $10.00$ ) spectrum showing signal annotations from leaves of *Berberis laurina* (400 MHz,  $\sim 10$  mg swollen in  $40\text{-}\mu\text{L}$   $\text{CD}_3\text{OD}$ ).

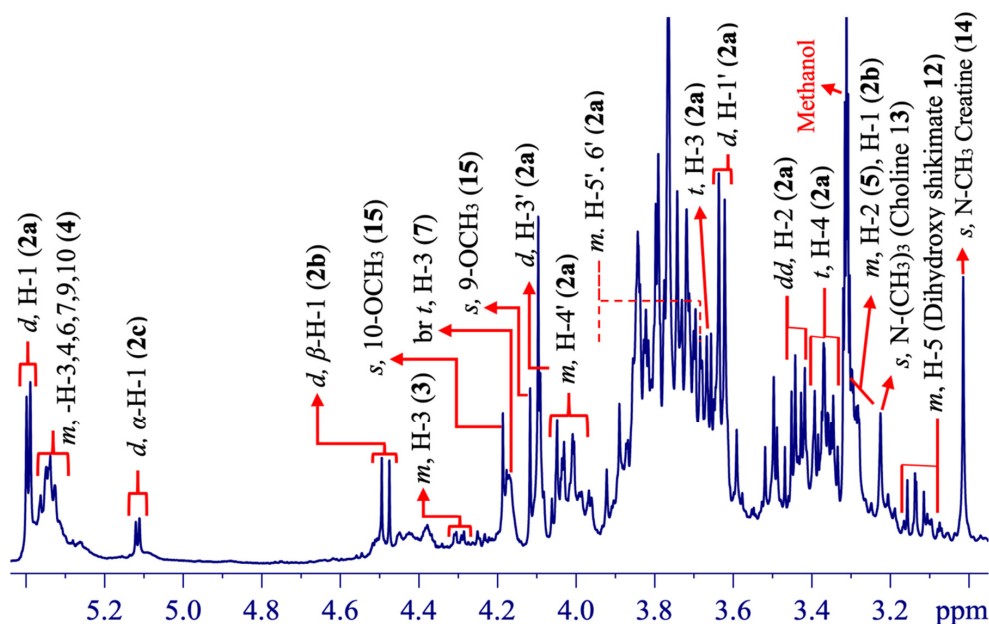


**Figure 5.**  $^1\text{H}$  HR-MAS NMR ( $\delta$  2.90–5.45) spectrum showing signal annotations from the leaves of *Berberis laurina* (400 MHz,  $\sim 10$  mg swollen in 40- $\mu\text{L}$   $\text{CD}_3\text{OD}$ ).

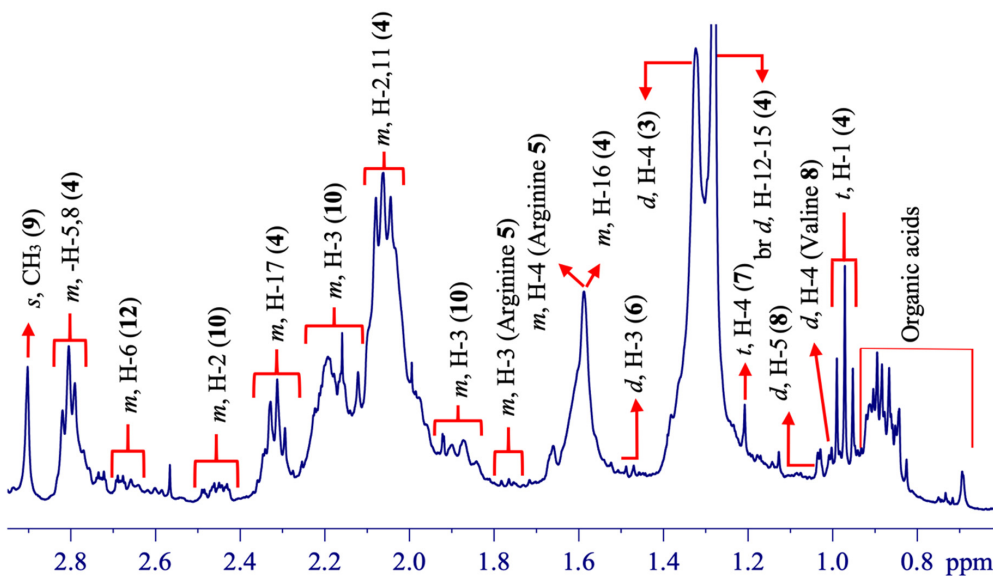


**Figure 6.**  $^1\text{H}$  HR-MAS NMR ( $\delta$  0.67–2.96) spectrum showing signal annotations from the leaves of *Berberis laurina* (400 MHz,  $\sim 10$  mg swollen in 40- $\mu\text{L}$   $\text{CD}_3\text{OD}$ ).

In the aromatic region of the spectrum (Figure 4), three chemical components, caffeic acid (1), fumaric acid (11), and berberine (15), with additional signals from other compounds (i.e., arginine 5 and dihydroxy shikimate 12), were observed.

Caffeic acid (1) was detected due to its typical two doublet signals with larger and equal magnitudes of scalar ( $J$ ) couplings representing a *trans*-configuration in the system; one was at  $\delta$  7.55 (d,  $^3J_{\text{H-H}} = 15.9$  Hz, H-7), and the second was at  $\delta$  6.27 (d,  $^3J_{\text{H-H}} = 15.9$  Hz, H-8), assigned to the hydrogens on positions 7 and 8 [36]. An intense doublet signal of a small  $J$ -coupling at  $\delta$  7.04 (d,  $^4J_{\text{H-H}} = 1.9$  Hz, H-2) was assumed to be an aromatic H-2 *meta*-coupled to H-6 revealed by a double doublet at  $\delta$  6.95 (dd,  $^3,^4J_{\text{H-H}} = 8.1; 1.9$  Hz, H-6). Its splitting pattern showed that it was still *ortho*-coupled to H-5 exposed via a doublet at  $\delta$  6.76 (d,  $^3J_{\text{H-H}} = 8.1$  Hz, H-5) in the molecular system of 1. The entire signal assignments for 1 were confirmed based on 2D NMR experiments performed in solution state

(Figures S3–S11), as well as previous reported data [36]. Caffeic acid (**1**) is a characteristic metabolic component of the phenylpropanoid or lignin biosynthetic pathway in plants [37,38]. It is chemically a functional metabolite in the plant itself as an antipredator agent, nascent leaves protector, and growth developer, as well as antioxidant, anti-inflammatory, and antiviral and functional in cardiovascular and diabetes diseases [37]. It has been previously described in *Berberis aristata* DC., a plant from the same family of *B. laurina* Billb. [39].

Fumaric acid (**11**) [40] was detected through a typical singlet signal at  $\delta$  6.54 (s, H-2, and 3), representing both hydrogens at positions 2 and 3 in the molecule. It is a small organic compound involved in the tricarboxylic acid cycle as a basic component for energy storage, and consumed in the biosynthesis of other molecules in plants [41]. This small organic acid is generally used as an additive and antioxidant agent in food products and useful as anti-inflammatory and antibacterial [42,43].

Berberine (**15**), a main alkaloid compound, was identified based on several singlet signals in the high-frequency range of  $\delta$  9.67 (s, H-8) and  $\delta$  8.56 (s, H-13) [44]. Moreover, two individual doublets of equal  $J$ -coupling constants were observed in the  $\delta$  8.05 (d,  $^3J_{\text{H-H}} = 9.1$  Hz, H-11), representing H-11, *ortho*-coupled to H-12, that appeared at  $\delta$  7.93 (d,  $^3J_{\text{H-H}} = 9.1$  Hz, H-12) on the aromatic site in **15**. Additionally, one of the two individual singlets was revealed at  $\delta$  7.64 (s, H-1) and the other singlet signal at  $\delta$  6.99 (s, H-4). Likewise, a singlet was revealed at  $\delta$  6.09 (s), which was assigned to two hydrogen nuclei in a methylene group directly connected to two oxygen atoms (-O-CH<sub>2</sub>-O-). The remaining signals were observed in another segment of the spectrum (Figure 5) at  $\delta$  4.11 (s) and 4.18 (s) which were assigned to methoxy hydrogens (-OCH<sub>3</sub>) on positions 9 and 10, respectively. Similarly, the remaining two signals (triplets) were in a highly crowded region of the spectra and were not observed. The entire signal assignments (with minor distinctions in chemical shifts) for **15** were comparative to those in the spectrum recorded from the roots (also stems) of *B. laurina* that provided all signals at higher intensities (discussed below) and were in accordance with those in previously published data [44]. The berberine compound has been identified in the literature, although using several pretreatment sequences such as extraction, isolation, and purification and, so, characterized through some spectroscopic and spectrometric approaches [45]. Additional reports highlighted the presence of alkaloids, terpenoids, flavonoids, sterols, anthocyanins, lignans, vitamins, proteins, lipids, and carotenoids in multiple *Berberis* genera from Berberidaceae [1].

The second segment of the spectrum (Figure 5) showed several superimposed signals related to various chemical components such as carbohydrates (sucrose (**2a**),  $\beta$ -glucose (**2b**),  $\alpha$ -glucose (**2c**)), threonine (**3**), fatty acids (**4**), arginine (**5**), 3-hydroxybutyric acid (**7**), dihydroxy shikimate (**12**), choline (**13**), creatine (**14**), and some signals from berberine (**15**).

The presence of sucrose (**2a**),  $\beta$ -glucose (**2b**), and  $\alpha$ -glucose (**2c**) were confirmed based on their typical anomeric hydrogen signals, such as doublets at  $\delta$  5.38 (d,  $^3J_{\text{H-H}} = 3.8$  Hz,  $\alpha$ -H in glucose unit),  $\delta$  4.47 (d,  $^3J_{\text{H-H}} = 7.8$  Hz,  $\beta$ -H), and  $\delta$  5.12 (d,  $^3J_{\text{H-H}} = 3.7$  Hz,  $\alpha$ -H). The assignments of carbohydrate contents (**2a–c**) were, in comparison to the published data, acquired in methanolic extracts of *Citrus*-type crude drugs of Kijitsu, Touhi, Chimpi, Kippi, and Seihi botanical materials [46]. Carbohydrate contents were essentially distributed and considered the main sources of energy in plants, as evidenced in roots of *Berberis chitria* Buch.-Ham. ex Lindl. of same family Berberidaceae [45].

Threonine (**3**) was detected by a broad and less intense multiplet signal in the range of  $\delta$  4.29 (*brm*, H-3) [47]. Threonine is a primary metabolite, principal growth regulator and defender in drastic conditions, as well as a nutritional needs promoter in plants [48,49]. A further primary metabolite, the fatty acid (**4**), was detected by certain signals of vinylic hydrogen nuclei appeared at  $\delta$  5.34 (m, H-3, 4, 6, 7, 9, and 10) [50,51]. Choline (**13**) was observed by a singlet signal for N-(CH<sub>3</sub>)<sub>3</sub> at  $\delta$  3.20 (s) [40] and 3-hydroxybutyric acid (**7**) [47] at  $\delta$  4.18 (*brs*, H-3), plus an additional broad signal at  $\delta$  1.21 (*brs*, H-4) in Figure 5. Alanine (**6**) was detected by a doublet at  $\delta$  1.48 (d,  $^3J_{\text{H-H}} = 7.20$  Hz, H-3) [52], dihydroxy shikimate (**12**) was observed (Figures 4–6) by a singlet at  $\delta$  6.38 (s, H-2), and two multiplets at  $\delta$  3.10 (m, H-5) and  $\delta$  2.66 (m, H-6) [40].

The singlet signal at  $\delta$  3.02 (s, 3H) (Figure 5) was assigned to the N-CH<sub>3</sub> methyl group of creatine (14). Although this assignment should be carefully evaluated, since creatine is not considered a compound from the kingdom plantae. There are only few reports, such as in *Phaseolus mungo* (L.) Hepper, *Lens culinaris* Medik., and *Eugenia uniflora* L. [53,54]. Even though, it is remarkably interesting to notice that this same NMR singlet signal was previously described only in *Eugenia uniflora* L. [19,54]. In several works regarding plant tissue investigations through HR-MAS NMR approach, any singlet signal has been described around  $\delta$  3.02 ppm, excepting for *Eugenia uniflora* L. and, now, *Berberis laurina* Billb.

In addition the third spectral part (Figure 6) showed several signals from fatty acids (4), arginine (5), alanine (6), 3-hydroxybutyric acid (7), valine (8), trimethylamine (9), and glutamic acid (10), correspondingly.

The fatty acids (4) were confirmed specifically based on a triplet at  $\delta$  0.97 ( $^3J_{H-H} = 7.6$  Hz) of a linolenic acid counterpart [50,55]. The presence of this fatty acid chain would be suggested as one of the fatty acid acyl chains that constitute the lipophilic membrane of leaves and plays an integral defensive function in oxiredution processes during biochemical cycles of vegetal. Arginine (5) was characterized by multiplets observed in both spectral regions (Figures 4–6) by  $\delta$  3.27 (m, H-2), 1.77 (m, H-3), 1.60 (m, H-4), and 1.92 (m, H-5). Similarly, valine (8) was identified by a doublet signal at  $\delta$  1.03 (d,  $^3J_{H-H} = 2.7$  Hz, H-5), trimethylamine (9) by a singlet at  $\delta$  2.90 (s, N-(CH<sub>3</sub>)<sub>3</sub>), and glutamic acid (10) by multiplets at  $\delta$  2.45 (m, H-2) and 2.0 (m, H-3). In addition, certain signals were observed for already mentioned metabolites declared relatively in the previous spectral ranges (Figure 5). Chemical compounds such as arginine (5), alanine (6), and 3-hydroxybutyric acid (7) were previously observed in mangos during fruit developmental processes [47]. The other primary metabolites such as threonine (3), valine (8), trimethylamine (9), glutamic acid (10), dihydroxy shikimate (12), and choline (13) were previously reported in *Commiphora wightii* [40].

The overall NMR chemical shifts, coupling constants, and related literature to the chemical compounds (1 to 15) are shown in Table 1, as well as associated 2D NMR correlation maps are correspondingly given (Figures S3–S11).

**Table 1.** High-Resolution Magic Angle Spinning Nuclear Magnetic Resonance (HR-MAS NMR) chemical shift assignments of all metabolites detected in leaves, roots, and stems of *Berberis laurina* Billb. (Berberidaceae).

Compound	Position	Current Work <sup>a</sup>			Literature <sup>b</sup>	
		$\delta_H$ (mult. J, Hz)	$\delta_C$	$^{LR}J_{H-C}$ (HMBC)	$\delta_H$ (mult. J, Hz)	$\delta_C$
Caffeic Acid (1)	1	-	127.8	-	-	127.2
	2	7.04 (d, 1.9)	115.2	149.5; 147.0; 122.7	7.07 (d, 2)	114.1
	3	-	147.0	-	-	145.5
	4	-	149.5	-	-	148.5
	5	6.76 (d, 8.1)	116.3	149.5; 147.0; 127.8; 122.7	6.77 (d, 7.8)	115.2
	6	6.95 (dd, 8.1; 1.9)	122.7	149.5; 115.2	6.95 (dd, 7.9; 1.9)	121.7
	7	7.55 (d, 15.9)	146.8	168.8; 122.7; 115.2	7.62 (d, 16.1)	145.7
	8	6.27 (d, 15.9)	115.2	168.8; 127.8	6.42 (d, 16.1)	115.0
	9	-	168.8	-	-	167.8
Sucrose (2a)	$\alpha$ -H-1	5.38 (d, 3.8)	93.4	105.4; 74.5	5.37 (d, 3.8)	95.4
	2	3.42 (dd, 9.8; 3.8)	74.5	74.8	3.40 (dd, 9.8; 3.8)	75.0
	3	3.70 (t, 9.5)	74.8	71.3	3.68 (t, 9.6)	76.4
	4	3.36 (t, 9.5)	71.3	74.8; 71.6; 62.1	3.34 (t, 9.4)	73.0
	5	-	-	-	-	76.1
	6	-	-	-	3.70 (dd, 7.9; 4.0)	63.9
	1'	3.62 (d, 5.1)	63.8	105.4; 79.2	3.58 (d, 12.3)	65.7
	2'	-	105.4	-	-	107.1
	$\beta$ -H-3'	4.10 (d, 8.3)	79.2	75.6; 63.8	4.08 (d, 8.2)	81.0
	4'	4.0 (m)	75.6	63.4	4.01 (t, 7.7)	77.4
	5'	3.69-3.87 (m)	83.9	83.9; 75.6	3.72-3.83	85.6
	6'	-	63.4	-	3.83-3.72	65.1

Table 1. Cont.

Compound	Position	Current Work <sup>a</sup>			Literature <sup>b</sup>	
		$\delta_H$ (mult. <i>J</i> , Hz)	$\delta_C$	$^{LR}J_{H-C}$ (HMBC)	$\delta_H$ (mult. <i>J</i> , Hz)	$\delta_C$
$\beta$ -glucose (2b)	$\beta$ -H-1	4.47 (d, 7.8)	98.2	-	4.45 (d, 7.8)	99.99
	2	3.11 (d, 7.8)	77.9	-	-	78.1
	3	-	74.6	-	-	79.8
	4	-	77.9	-	-	72.2
	5	-	74.6	-	-	79.9
	6	-	-	-	-	64.6
$\alpha$ -glucose (2b)	$\alpha$ -H-1	5.12 (d, 3.7)	93.5	-	5.09 (d, 3.7 Hz)	95.7
	2	3.36 (d, 3.7)	71.4	-	-	-
	3	-	-	-	-	-
	4	-	-	-	-	-
	5	-	-	-	-	-
	6	-	-	-	-	-
Threonine (3)	1	-	-	-	-	-
	2	-	-	-	3.51 (d, 12.0)	-
	3	4.29 ( <i>br</i> , <i>m</i> )	-	-	4.27 ( <i>m</i> )	-
	4	1.32 (d, 7.0)	30.2	-	1.32 (d, 7.0)	-
Fatty Acids (4)	1	0.97 (t, 7.6)	18.3	132.8	0.95 (t, 7.5)	-
	2, 11	2.1 ( <i>m</i> )	28.1	129.2; 30.8	-	-
	-HC = CH-	5.34 ( <i>m</i> )	129.3\72.0	26.6	-	-
	5, 8	2.81 ( <i>m</i> )	26.3	129.2; 44.1	-	-
	12-15	1.30 ( <i>br</i> , <i>d</i> )	30.5	30.5	-	-
	16	1.60 ( <i>m</i> )	26.1	30.5	-	-
	17	2.32 ( <i>m</i> )	35.2	174.8; 30.5; 26.1	-	-
	18	-	174.8	-	-	-
Arginine (5)	1	-	-	-	-	-
	2	3.27 ( <i>m</i> )	71.4	-	3.25	-
	3	1.77 ( <i>m</i> )	-	-	1.77	-
	4	1.60 ( <i>m</i> )	26.0	-	1.59	-
	5	1.92 ( <i>m</i> )	38.7	-	1.91	-
	6	-	-	-	-	-
Alanine (6)	1	-	-	-	-	-
	2	-	-	-	-	-
	3	1.48 (d, 7.20)	-	-	1.48 (d, 7.20)	-
3-hydroxybutyric acid (7)	1	-	-	-	-	-
	2	-	-	-	-	-
	3	4.18 ( <i>brs</i> )	-	-	4.19	-
	4	1.21 ( <i>brs</i> )	-	-	1.20	-
Valine (8)	1	-	-	-	-	-
	2	-	-	-	-	-
	3	-	-	-	2.27 ( <i>m</i> )	-
	4	-	-	-	0.99 ( <i>d</i> )	-
	5	1.03 (d, 2.7)	-	-	1.04 ( <i>d</i> )	-
Trimethylamine (9)	1	2.90 ( <i>s</i> )	40.2	-	2.89 ( <i>s</i> )	-
Glutamic acid (10)	1	-	-	-	-	-
	2	2.45 ( <i>m</i> )	-	-	2.37 ( <i>m</i> )	-
	3	2.0 ( <i>m</i> )	-	-	-	-
Fumaric acid (11)	2,3	6.54 ( <i>s</i> )	120.9	-	6.52 ( <i>s</i> )	-
Dihydroxy shikimate (12)	1	-	-	-	-	-
	2	6.38 ( <i>s</i> )	115.4	127.8	6.39 ( <i>s</i> )	-
	3	-	-	-	-	-
	4	-	127.8	-	-	-
	5	3.15-3.08 ( <i>m</i> )	71.1	-	3.07 ( <i>m</i> )	-
	6	2.66 ( <i>m</i> )	63.5	192.5	2.62 ( <i>m</i> )	-
	7	-	192.5	-	-	-
Choline (13)	1	3.22 ( <i>s</i> ) N-(CH <sub>3</sub> ) <sub>3</sub>	55.0	77.8; 55.0	3.21 ( <i>s</i> ) N-(CH <sub>3</sub> ) <sub>3</sub>	-
	2	-	77.8	-	-	-
	3	-	-	-	-	-
Creatine (14)	-	3.02 ( <i>s</i> ) N-CH <sub>3</sub>	43.9	-	-	-

Table 1. Cont.

Compound	Position	Current Work <sup>a</sup>			Literature <sup>b</sup>	
		$\delta_{\text{H}}$ (mult. <i>J</i> , Hz)	$\delta_{\text{C}}$	$^{\text{LR}}J_{\text{H-C}}$ (HMBC)	$\delta_{\text{H}}$ (mult. <i>J</i> , Hz)	$\delta_{\text{C}}$
Berberine (15)	1	7.63 (s)	107.7	152.1; 149.9; 139.6; 131.8	7.45 (s)	106.5
	2	-	152.1	-	-	152
	2,3-OCH <sub>2</sub> O	6.11 (s)	104.7	152.1; 149.9	6.13 (s, -OCH <sub>3</sub> )	103.6
	3	-	149.9	-	-	149.9
	4a	-	121.8	-	-	121.9
	4	6.96 (s)	110.7	152.1; 149.9; 121.8; 28.6	6.89 (s)	109.3
	5	3.26 (t, <i>J</i> = 6.3 Hz)	28.6	131.8; 121.8; 110.7; 58.3	3.26 (t, 5.6 Hz)	28.2
	6	4.92 (t, <i>J</i> = 6.3 Hz)	58.3	147.3; 139.6; 131.8; 28.6	4.95 (t, 5.6)	57.1
	7	-	-	-	-	-
	8a	-	135.3	-	-	135.1
	8	9.74 (s)	147.3	145.8; 139.6; 135.3; 58.3	9.78 (s)	146.4
	9	-	145.8	-	-	145.7
	H <sub>3</sub> CO-9	4.11 (s)	58.8	152.0	4.12 (s, -OCH <sub>3</sub> )	54.6
	10	-	152.0	-	-	152
	H <sub>3</sub> CO-10	4.20 (s)	63.6	145.8	4.35 (s, -OCH <sub>3</sub> )	62.5
	11	8.11 (d, 9.1 Hz)	129.3	145.8; 135.3	8.00 (d, 7.98 Hz)	128
	12a	-	123.3	-	-	123.3
	12	8.0 (d, 9.1 Hz)	125.4	152.0; 123.3	7.95 (d, 7.98 Hz)	124.5
13	8.65 (s)	122.7	139.6; 125.4; 123.3; 122.7	8.61 (s)	121.5	
14a	-	131.8	-	-	131.9	
14	-	139.6	-	-	139.6	

$\delta_{\text{H}}$  = <sup>1</sup>H Nuclear Magnetic Resonance chemical shift,  $\delta_{\text{C}}$  = <sup>13</sup>C Nuclear Magnetic Resonance chemical shift, (mult. *J*, Hz) = Multiplicity and coupling constants in Hertz,  $^{\text{LR}}J_{\text{H-C}}$  (HMBC) = Long-range <sup>1</sup>H-<sup>13</sup>C correlation from Heteronuclear Multiple-Bond Correlation. <sup>a</sup> Experimental work, acquired at 400 and 100-MHz for <sup>1</sup>H and <sup>13</sup>C, respectively, from swollen materials in CD<sub>3</sub>OD containing TMS (*v/v*, 0.05%) as the internal reference. (1)<sup>b</sup> <sup>1</sup>H 500.13 and <sup>13</sup>C 125.75 MHz in CD<sub>3</sub>OD [36]; (2a-c)<sup>b</sup> <sup>1</sup>H 800 and 201 MHz for <sup>1</sup>H and <sup>13</sup>C in CD<sub>3</sub>OD [46]; (3)<sup>b</sup>, (5)<sup>b</sup>, (7)<sup>b</sup>, and (8)<sup>b</sup> <sup>1</sup>H 500.13-MHz in CD<sub>3</sub>OD, KH<sub>2</sub>PO<sub>4</sub> in D<sub>2</sub>O and TSP [47]; (4)<sup>b</sup> <sup>1</sup>H 500.13-MHz in CD<sub>3</sub>OD, KH<sub>2</sub>PO<sub>4</sub> in D<sub>2</sub>O and TSP [51]; (6)<sup>b</sup> <sup>1</sup>H 500.13 MHz in CD<sub>3</sub>OD + phosphate buffer in D<sub>2</sub>O [52]; (9)<sup>b</sup>, (10)<sup>b</sup>, (11)<sup>b</sup>, (12)<sup>b</sup>, and (13)<sup>b</sup> <sup>1</sup>H 800-MHz in D<sub>2</sub>O and TSP [40]; and (14)<sup>b\*</sup> and (15)<sup>b</sup> <sup>1</sup>H 400: <sup>13</sup>C 100-MHz CD<sub>3</sub>OD [44]. The respective multiplicities are shown with the letters “s” (singlet), “d” (doublet), “t” (triplet), and “m” (multiplet). b\* = confirmed with online databases.

## 2.2. <sup>1</sup>H HR-MAS NMR-Based Chemical Composition of Stems and Roots of *Berberis laurina*

In same way, the stems and roots of *Berberis laurina* Billb. were analyzed through HR-MAS NMR spectroscopy in their natural, unaltered states. In comparison to leaves, the HR-MAS NMR spectra of the stems and roots presented less overlapped NMR spectra, which are associated with high-intense signals, mainly in those from the roots (Figure 7).

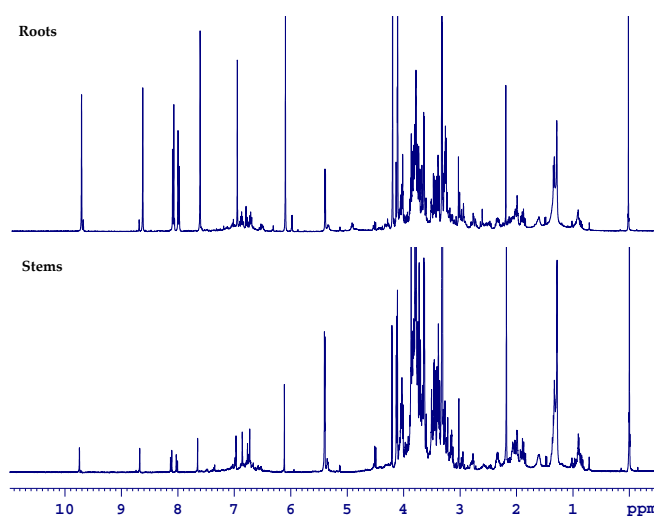


**Figure 7.** Comparative overview of <sup>1</sup>H HR-MAS NMR spectra ( $\delta$  −0.50–11.00) from the roots and stems parts of *Berberis laurina* (400 MHz, ~10 mg swollen in 40  $\mu$ L CD<sub>3</sub>OD).

In this case, to facilitate the chemical compositional overview for the roots and stems, the spectra were divided into two sections: the high frequency comprising aromatic and olefinic signals and low frequency containing aliphatic ones (Figures 8 and 9).

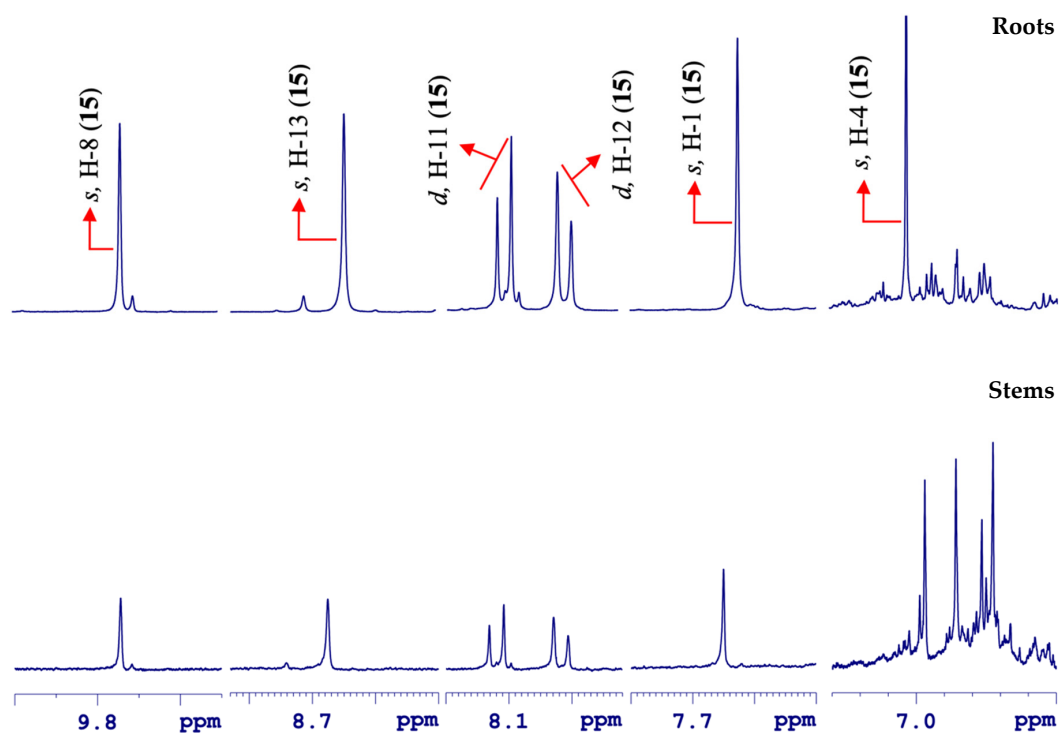


**Figure 8.** Comparative overview of the amplified aromatic region in the  $^1\text{H}$  HR-MAS NMR spectra from the roots and stems parts in *Berberis laurina* (400 MHz, ~10 mg swollen in 40  $\mu\text{L}$   $\text{CD}_3\text{OD}$ ).

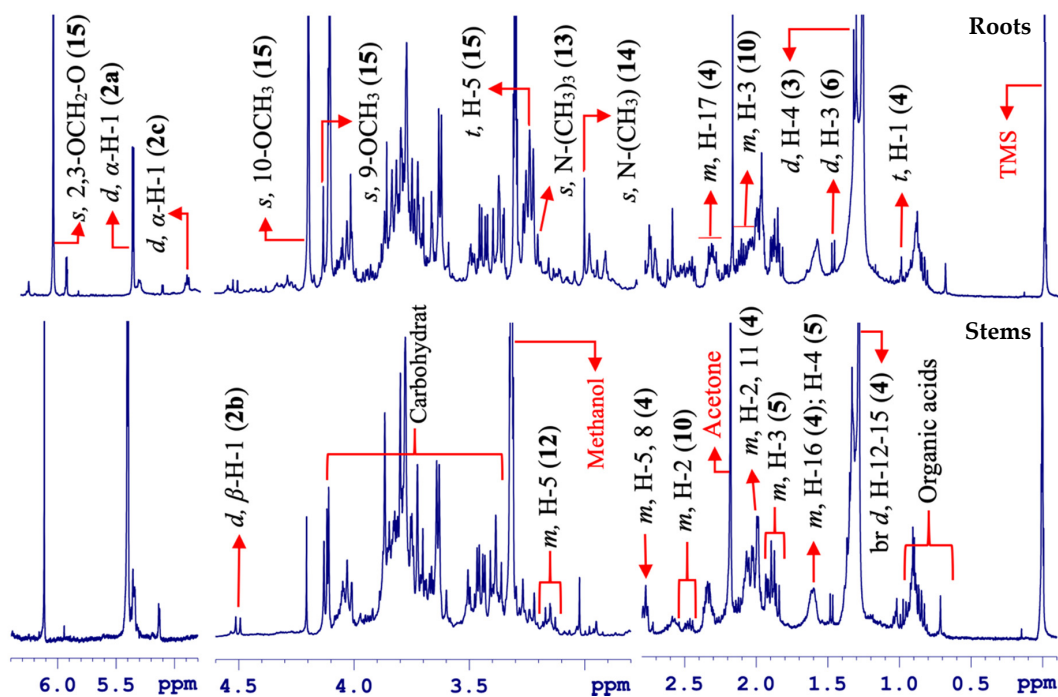


**Figure 9.** Comparative overview of the amplified olefinic, carbohydrates, and aliphatic regions in the  $^1\text{H}$  HR-MAS NMR spectra from the roots and stems of *Berberis laurina* (400 MHz, ~10 mg swollen in 40- $\mu\text{L}$   $\text{CD}_3\text{OD}$ ).

Berberine (**15**) was initially observed through two singlet signals at  $\delta$  9.74 (s, H-8) and 8.65 (s, H-13) [44]. Furthermore, two doublets of equal  $J$ -coupling constants were observed at  $\delta$  8.11 (d,  $^3J_{\text{H-H}} = 9.1$  Hz, H-11) and 8.00 (d,  $^3J_{\text{H-H}} = 9.1$  Hz, H-12) from two mutually *ortho*-coupled hydrogen nuclei on the aromatic ring in the molecule. Additionally, other intense singlets appeared at  $\delta$  7.63 (s, H-1) and 6.96 (s, H-4) (Figure 8).

Similarly, the remaining singlets at  $\delta$  6.11 (s), 4.20 (s, 3H), and 4.11 (s, 3H) from hydrogen nuclei in the 2-O-CH<sub>2</sub>-O-3, H<sub>3</sub>CO-10, and H<sub>3</sub>CO-9 groups were observed in the aliphatic region. Likewise, two individual triplets of equal  $J$ -coupling magnitudes were found at  $\delta$  4.92 (t,  $^3J_{\text{H-H}} = 6.3$  Hz, H-5) and 3.26 (t,  $^3J_{\text{H-H}} = 6.3$  Hz, H-6), which were mutually coupled due to their coupling patterns and were assigned to H-5 and H-6 (Figure 9).

According to the previous studies, berberine is an alkaloid of strongly yellow color and active as an antifungal, antibacterial, antiviral, cardiovascular, anti-inflammatory, antidiabetes, and other biological activities [56]. The findings from this work allowed to realize that the roots followed by stems of *Berberis laurina* are a rich natural source for the alkaloid berberine (**15**). On the other hand, the aerial parts are an interesting source for caffeic acid.

Other than berberine (**15**), the carbohydrate contents included sucrose (**2a**), which was perceived by means of distinct doublets at  $\delta$  5.40 (d,  $^3J_{\text{H-H}} = 3.8$  Hz, H-1 in the glucose unit), the  $\beta$ -glucose (**2b**) by the signal at  $\delta$  4.51 (d,  $^3J_{\text{H-H}} = 7.8$  Hz,  $\beta$ -H), and also,  $\alpha$ -glucose (**2c**) by a representative doublet at  $\delta$  5.14 (d,  $^3J_{\text{H-H}} = 3.7$  Hz,  $\alpha$ -H). Less intense signals were observed for vinylic hydrogen nuclei at  $\delta$  5.34 (m) and  $\delta$  1.28 of methylene (CH<sub>2</sub>) of fatty acids (**4**), with an additional singlet signal at  $\delta$  3.02 (s) for creatine (**14**) in the fresh roots and stems of *B. laurina*.

Additionally, the confirmation of all identified chemical compounds in all three parts (leaves, stems, and roots) were based on HR-MAS followed by 2D NMR experiments in a liquid state (Figures S3–S11) and the literature data, as well as online databases such as MetaboLights available at <https://www.ebi.ac.uk/metabolights/index> and the Biological Magnetic Resonance Data Bank, BMRB, which can be accessed at <http://www.bmrwisc.edu/>. An overview of the complete details related to the identified metabolites in *Berberis laurina* are presented in Table 1.

### 2.3. <sup>1</sup>H HR-MAS NMR-Based Insight into the Leaves Metabolic Patterns

Plants are natural resources to produce manifold small organic compounds, covering intermediates to final products of multiple intracellular biosynthetic events, which are closely associated to the environmental conditions [32,57]. These small chemical entities are primary and secondary metabolites of distinctive classes of carbohydrates, organic and fatty acids, terpenoids, alkaloids, and phenolic compounds that have several functional properties [29,32,33]. Metabolites are crossing points between plant and environmental trends that are main stimuli to the usual life stages and affective towards the metabolic patterns, as seen in different parts (roots, stems, leaves, and flowers) of several plants [32,58].

To study the metabolic pattern (or fingerprints) associated to the environment and periodical flux, HR-MAS NMR-based fingerprinting analyses were applied to follow the chemical compositions over the time, as well as according to plant topology. In such, the HR-MAS NMR approach was applied to the top, middle, and bottom of *Berberis laurina* during a period of seven months (October 2018 to April of 2019). The quantitative levels of chemical compounds could be traced directly from its HR-MAS NMR spectra. Indeed, the signal intensities were proportional to the amount of chemical compounds in the materials. The plant was cultivated in an open environment, meaning that it was totally exposed to environmental (a)biotic communications.

The visual inspection of HR-MAS NMR spectra disclosed most of the intense signals in the middle leaves, followed by the top and bottom. Substantial increases in the signals' relative intensities were observed for caffeic acid (**1**), sucrose (**2a**),  $\beta$ -glucose (**2b**),  $\alpha$ -glucose (**2c**), and creatine (**14**) metabolites (Figure 10). On the other hand, screening the same spectra in accordance to the fluctuated period (months), manifold signal intensifications could be observed frequently in all metabolites during October 2018 (Spring) and April 2019 (Fall). The quantitative (de)escalation in the plant metabolic

profiles was supposed to be due to the interlinked environmental effects on the chemical substances, which have been previously described for other plants [32,59,60].

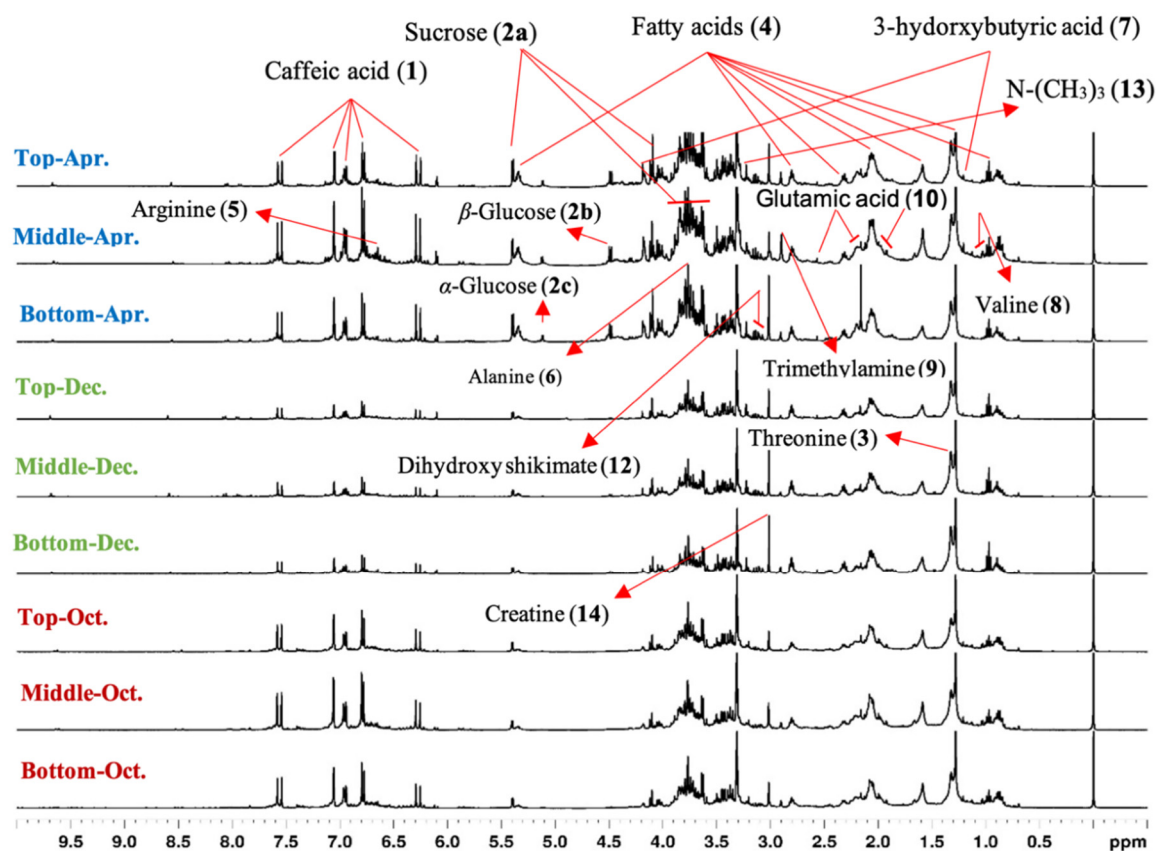


**Figure 10.** Stacked outline and visual assessment of the  $^1\text{H}$  HR-MAS NMR spectra recorded from the leaves of *Berberis laurina* associated to different times (October 2018 to April 2019).

The comparative spectral profiles (October 2018 to April 2019) demonstrated that those signals for caffeic acid (1) were of high intensities in October 2018, while they were downregulated in December 2018 and again upregulated in April 2019 (Figure 10). According to the climate data, November and December 2018 experienced a meaningful reduction in rainfall precipitation, as well as temperatures that started to increase, with the highest one in December 2018 (Figure S12). This means that caffeic acid production may be correlated to water scarcity, or its need decreases in low precipitation seasons. In a holistic overview regarding all seven months (October 2018 to April 2019), it was observed that bottom leaves presented only a small higher average production of caffeic acid (1), although they presented the higher dispersion over the time, as well (Figure S13).

The signals for sugar components sucrose (2a),  $\beta$ -glucose (2b), and  $\alpha$ -glucose (2c) were of high intensities in April 2019. In March and April 2019, the temperatures started to decrease as well as a reduction in rainfall precipitation was experienced (Figure S12). Although, this correlation must be noticed carefully, since both of them presented relatively high content dispersions over the time, no matter the plant topology (Figure S13).

These up- (and or down) regulations in signal intensities indicate a significant dependence on the environmental conditions, such as rainfall, solar indices, and seasonal and temperature changes [32,59,60].

#### 2.4. Principal Component Analysis-Based Metabolic Pattern Discrimination in the Leaves

The comprehensive details regarding the molecular pattern fluctuations revealed by HR-MAS NMR analysis may be furthermore streamlined through multivariate statistical analysis by means of

principal component analysis (PCA) [12,61]. In this, features can be retained when multidimensional HR-MAS NMR raw data is mathematically transformed into readable small-dimensional variables, the principal components (PCs). In turns, the main objective performing PCA was to follow the changes in the chemical compositions of aerial parts *Berberis laurina* over the time (month-wise) in a smart way.

As described previously (see Section 2.3), the plant topology was associated to the leaves (top, middle, and bottom). The NMR experiments were conducted in triplicate ( $n = 3 \times 9$ ) under the same and uniform experimental conditions. PCA was performed with the aid of a Bruker AMIX software package to a selected spectral range ( $\delta$  0.60–10.00), excluding unwanted regions such as the residual water signal ( $\delta$  4.73–5.00), as well as acetone ( $\delta$  2.14–2.16) and partially deuterated methanol ( $\delta$  3.29–3.32) residual signals. First of all, the  $^1\text{H}$  MHR-MAS NMR spectra were converted in buckets (binning) by dividing the spectral width into equal small segments 0.04-ppm wide, resulting in a  $X$ -sized bucket table equivalent to 28 rows containing NMR spectra (i.e., samples) vs. 174 columns comprising the variables (i.e., NMR chemical shifts). In the generated buckets table, each relative intensity along the rows (i.e., spectra) was normalized based on the total spectral area, while, column-wise (i.e., variables), were submitted to pareto scaling. In contrast to autoscaling and no scale, the pareto scaling method is supposed to be beneficial, particularly in NMR-based fingerprinting approaches, which balance all nonuniform variables by avoiding expected noise and additional artifacts in the spectra [62,63]. In other words, autoscaling means that all columns (i.e., variables) are equally weighted during PCA, although it can overestimate those buckets containing noise. On the other hand, no scaling preserves the natural differences in intensities, although it highlights dominant effects such as high-intensity signals in detriment to those that have a low intensity. Pareto scaling is in between no scaling and autoscaling, without overestimating noisy variations by reducing the relative importance of intense buckets and keeping the data structure partially intact. In the mathematical sense, the pareto scale divides the mean centered variables by the square root of the standard deviation (SD) as a scaling function [4,64]. After normalization and scaling, PCA itself was performed at a confidence level of 95%, thus generating both score and loading plots. The PCA of the NMR spectra resulted in a net variance of 82.34% distributed in the first two principal components (PCs; PC1 = 50.25% vs. PC2 = 32.09%).

The inspection of the score plot permitted to visualize sample discriminations into three main groups or clusters over the time (October 2018, December 2018, and April 2019), although not between the leaf topology, instead (Figure 11). This means that the chemical variability in the course of time is higher than the variability due to the leaf topology. In other words, there is no highly significant differences in the chemical compositions of the top and bottom leaves. Rendering to the PCs, PC1 (50.25%) was responsible for the separation of the December 2018 and October 2018 samples, which were located along the negative and positive PC1, respectively, although both were along negative PC2. This found indicates that there a significant difference in the chemical composition of the leaves regarding the extreme periods (December to October), as previously observed by a visual inspection (see Section 2.3). On the other hand, the April 2019 samples were discriminated from the other groups only in PC2 (32.09%), being positive in PC2, although between positive and negative in PC1, which means they present a transition chemical composition.

The main chemical features responsible for group separations in the course of time were achieved by looking in the same direction of the loadings plot (Figure 12) resulting from the PCA. Throughout, December 2018 samples were separated mainly based on three metabolites: fatty acids (**4**), choline (**13**), and creatine (**14**). In such, due to variables (i.e., NMR chemical shifts) at  $\delta$  0.98/0.96–1.00 (t7.6 Hz, H-1), a characteristic signal from a methyl group ( $\text{CH}_3$ ) of fatty acids in the  $^1\text{H}$  NMR spectra, as well as signals at  $\delta$  2.30/2.28–2.32 (m, H-17); 2.82/2.80–2.84 (m, H-5 and 8); and  $\delta$  1.30/1.28–1.32 (*brs*, H-12, 13, 14, and 15) of all methylene groups ( $\text{CH}_2$ ) from the fatty acids (**4**). The main discriminatory variables for the two other metabolites were two singlets, one from choline (**13**) at  $\delta$  3.22\3.20–3.24 (s) regarding the methyl hydrogen nuclei in  $\text{N}-(\text{CH}_3)_3$  and the other from creatine (**14**) at  $\delta$  3.02\3.00–3.04 (s) for the hydrogen nuclei in a methyl group in  $\text{N}-\text{CH}_3$  in the molecular structure (Figure 12).

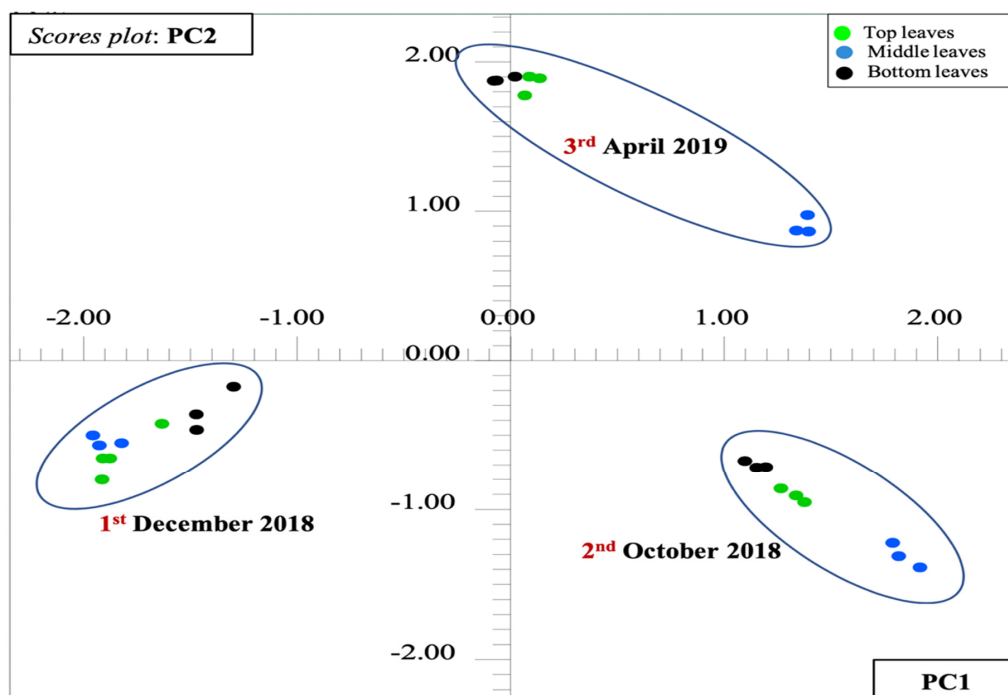


**Figure 11.** Scores plot from the principle component analysis (PCA) performed over  $^1\text{H}$  HR-MAS NMR spectra ( $\delta$  10.0–0.60, 0.04-ppm bucket size, and pareto-scaled) acquired directly from the leaves of *Berberis laurina* showing discrimination according to the season time. PC1 (50.25%) vs. PC2 (32.09%) of the  $28 \times 174$  data matrix that revealed a net variance of 82.34%.

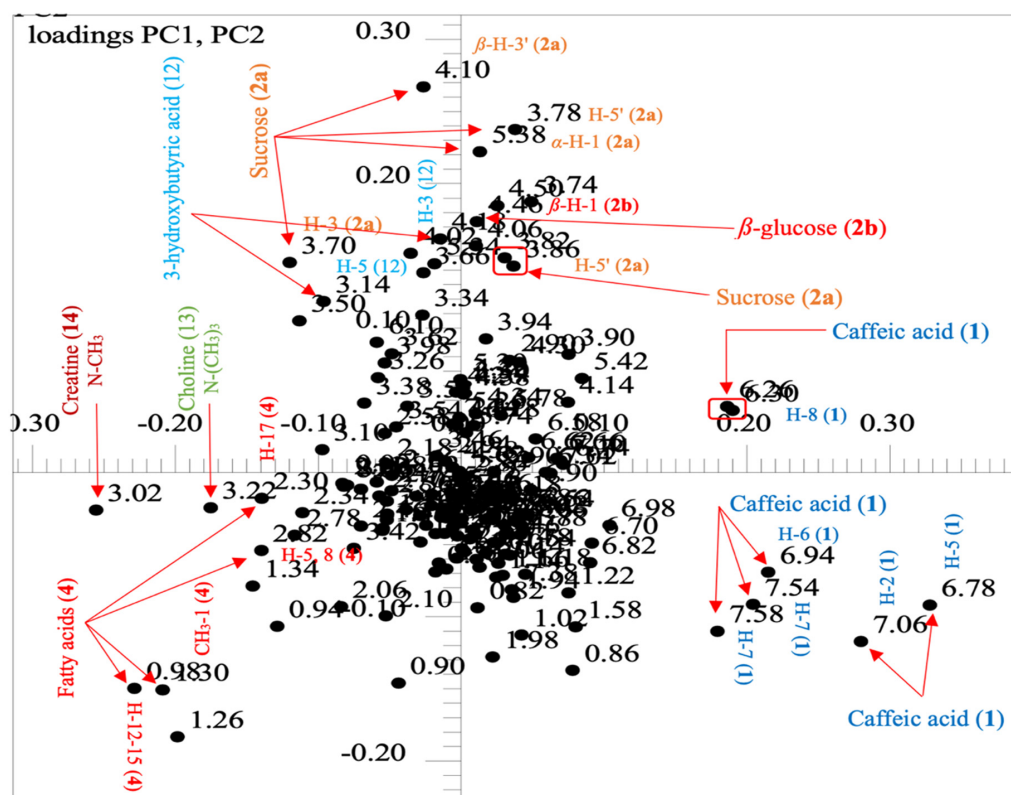


**Figure 12.** Loadings plot showing all chemical features for each group revealed in the scores plot, obtained with spectral widths of  $\delta$  10.0 to 0.60 utilizing the bucket size  $\delta$  0.04 and pareto-scaled PC1 (50.25%) vs. PC2 (32.09%) of  $28 \times 174$  data matrix that revealed a net variance of 82.34%.

In the same way, October 2018 samples were discriminated almost exclusively due to a central metabolite, caffeic acid (**1**), supporting the visual section of the spectra (Section 2.3). In such, several signals of caffeic acid (**1**) appearing in different NMR chemical shifts, such as those from a *trans*-configuration spin system at  $\delta$  7.58/7.56–7.60 (d 15.9 Hz, H-8), and its relative counterpart at  $\delta$  7.06/7.04–7.08 (d 1.9 Hz, H-2), as well as those at  $\delta$  6.78/6.76–6.80 (d 8.1 Hz, H-5) and  $\delta$  6.95/6.93–6.97 (dd 8.1 and 1.9 Hz, H-6) from two mutually *para*-coupled aromatic spin systems, were responsible for sample discriminations (Figure 12). Caffeic acid is functional metabolite including antipredator and leaf protector properties. Thus, its boost in biosynthesis may be associated by the need of plant defense purposes against microorganisms and other predators that increase with the humidity, since October 2018 was of high rainfall precipitation (Figure S12).

Finally, April 2019 samples were based on three molecular components: sucrose (**2a**),  $\beta$ -glucose (**2b**), and caffeic acid (**1**). Several NMR chemical shifts from **2a** at  $\delta$  5.38/5.36–5.40 (d 3.8 Hz,  $\alpha$ -H-1), 4.10/4.08–4.12 (d 8.3 Hz,  $\beta$ -H-3'), and 3.78/3.76–3.80 (m, H-5'), as well as the doublet at  $\delta$  4.47/4.45–4.49 (d 7.8 Hz,  $\beta$ -H-1) from **2b**, appeared to be the main ones responsible for sample discriminations in positive-PC2. On other hand, the remaining signals were from caffeic acid (**1**) in the range of  $\delta$  6.30/6.28–6.32 (d 15.9 Hz, H-8) from a hydrogen nuclei in *E*-configuration to H-7 in the molecular structure, correspondingly (Figure 12). By this, it can be concluded that the apices on caffeic acid (**1**) biosynthesis can be achieved during April to October, mainly in the later one.

Considering the weather conditions when samples were collected, it can be realized that there is a high correlation between group discriminations in the PCA and the season time. October 2018 was of high precipitation rates and low temperatures, while December 2018 presented high temperatures and a significant reduction in rainfall precipitation. April 2019 can be described as a transition period, with higher rainfall precipitation rates than December 2018 but lower than October. The same can be observed for the temperature; while December and October presented the highest and lowest temperatures, respectively, April was in between instead (Figure S12). This finding clearly supports that environmental conditions have significant influences on the chemical compositions in the leaves of *Berberis laurina*. Moreover, HR-MAS NMR proved to be a tool of choice in investigating plant tissues in their natural, unaltered states.

### 3. Experimental

#### 3.1. Botanical Materials

Leaves (top, middle, and bottom); stem; and root samples (Figure 1) of *Berberis laurina* Billb. (Berberidaceae) species were collected during October 2018 to April 2019 from an open atmosphere in the Botanical Garden of Curitiba (Coordinates 25°26'27" S, 49°14'24" W: 910 m high), Curitiba, PR, Brazil. The plant was equally exposed to environmental interactions such as sunlight, moisture, airstream.

The taxonomical identification of the species was completed in the Herbarium of the Botanical Garden of Curitiba, PR, Brazil, and voucher specimen was deposited under the number MBM 415083 (Figure S14). All collected botanical material samples, including healthy leaves, stems, and roots, were first washed under running water to remove contamination. Followed by root and stem samples directly stored under freezing temperatures ( $-18$  °C), while leaf samples were previously dried under circulating air for two days at an average temperature of 45 °C and then stored at  $-18$  °C. The overall botanical material was then submitted to HR-MAS and liquid-state two-dimensional (2D) NMR analyses.

#### 3.2. $^1\text{H}$ HR-MAS NMR

To achieve high-resolution  $^1\text{H}$  HR-MAS NMR spectra, the leaves, roots, and stems were frozen in liquid nitrogen in a mortar and then grinded separately with aid of a pestle. After that, around 10 mg of the powder was inserted into a 50- $\mu\text{L}$  zirconium oxide HR-MAS rotor followed by subjecting 40  $\mu\text{L}$  of deuterated methanol ( $\text{CD}_3\text{OD}$ , 99.8% D, TMS 0.05% (*v/v*)) (Cambridge Isotopes Laboratory, Cambridge,

MA, USA) for lock and shimming purposes. The botanical material in the HR-MAS rotor was mixed with solvent, and bubbles were removed with a syringe needle and homogenized; eventually, the rotor was tightly packed. Each individual sample was left in the solvent inside the HR-MAS rotor for about 15 min to swell and attain a gel-like state prior to HR-MAS NMR measurements.

$^1\text{H}$  HR-MAS NMR analyses were carried out on a Bruker AVANCE 400 NMR spectrometer (Bruker, Karlsruhe, Germany) operating at 9.4 Tesla ( $^1\text{H}$  = 400.13 MHz). The spectrometer was equipped with a four channel ( $^1\text{H}$ ,  $^{13}\text{C}$ ,  $^{15}\text{N}$ , and  $^2\text{H}$  (lock channel)) 4-mm HR-MAS probe with actively gradient field along the magic angle direction (Figure S15). The rotors were spun at 5 kHz under 296 K temperature. Similarly, radio frequency (RF) circuit was tuned-matched to the  $^{79}\text{Br}$  ( $\leq ^{13}\text{C}$  = 100 MHz) frequency by using standard material (KBr) and realized that the magic angle was matching ( $\theta = 54.74^\circ$ ). In the same way, the magnetic field ( $B_0$ ) was manually homogenized by adjusting Z,  $Z^3$ , X, XZ,  $XZ^2$ , and XYZ shim coils, and tuning-matching was performed to the hydrogen nuclei channel coil circuit to  $^1\text{H}$  frequency.

The  $^1\text{H}$  HR-MAS NMR experiments were performed with aid of the solvent suppression, *zgcppr* pulse sequence (Bruker library, Karlsruhe, Germany)), to manipulate the intense water resonance. Overall acquisition parameters used in *zgcppr* were included: free induction decay (FID) size (TD = 64 k data points), spectral width (SW = 8012.8 Hz), acquisition time (AQ = 4.09 s), FID resolution (FIDRES = 0.12 Hz), receiver gain (RG = 57), transmitter offset frequency (O1 = 1955.0 Hz), temperature (296 K), recycle delay (D1 = 1 s), presaturation power attenuation (p19 = 55 dB),  $90^\circ$  flip angle pulse of 5.63  $\mu\text{s}$ , and total utilized scans (NS = 256). All spectra were processed by applying an exponential window multiplication to the free induction decays (FIDs) using a Lorentzian line-broadening function (LB = 0.3) and zero-filled to 64 k data points.

### 3.3. Liquid-State (2D) NMR

Once the 1D NMR spectra acquired directly from in nature sample presented a high overlap of signals, the molecular structure identification in the samples were facilitated by performing 2D NMR experiments in a liquid state. For these, 300-mg powdered botanical material were weighed in a microcentrifuge tube (1000  $\mu\text{L}$ ) followed by an addition of 650- $\mu\text{L}$  deuterated methanol ( $\text{CD}_3\text{OD}$ ), sonicated (25  $^\circ\text{C}$ , 40 min), centrifuged (30 min), and eventually, the supernatant was transferred into a 5-mm NMR tube.

The 2D NMR analyses were carried out on a Bruker AVANCE III 400 NMR spectrometer (Bruker, Karlsruhe, Germany) operating at 9.4 Tesla ( $^1\text{H}$  = 400.13 MHz and  $^{13}\text{C}$  at 100.62 MHz). The spectrometer was equipped with a three-channel ( $^1\text{H}$ ,  $^2\text{H}$  (lock channel) and X-nucleus) 5-mm broad-band inverse detection probe with actively gradient field along z-direction.

The single bond ( $^1J_{\text{H-C}} = 145$  Hz) to long-range multiple bonds ( $^{\text{LR}}J_{\text{H-C}} = 8$  Hz) heteronuclear ( $^1\text{H}$ - $^{13}\text{C}$ ) correlation measurements were achieved through 2D multiplicity edited HSQC and HMBC NMR experiments. Additionally, the nearby and long-range homonuclear ( $^1\text{H}$ - $^1\text{H}$ ) correlation measurements were carried out by 2D COSY and TOCSY experiments. The importance of 2D multiplicity edited HSQC NMR was to simplify and differentiate CH and  $\text{CH}_3$  from  $\text{CH}_2$  groups in the molecules. The edited HSQC is an equivalent 2D pattern of the DEPT-135 experiment, which provides a multiplicities edition and correlation information to simplify intramolecular connections utilizing distinct phases (i.e., positive and negative phases). In this work, the blue (in the positive phase) represented CH and  $\text{CH}_3$ , whereas the red color (in the negative phase) denoted all  $\text{CH}_2$  groups in the molecular structures.

### 3.4. Multivariate Statistical Analysis

Prior to multivariate statistical analysis, spectra base lines and phases were manually adjusted, and the NMR chemical shifts were referenced against the TMS signal at  $\delta$  0.00, as the internal reference, with the aid of Topspin software (Bruker). After that, the  $^1\text{H}$  HR-MAS NMR spectra ( $\delta$  0.60–10.00, except those regions regarding residual water signals ( $\delta$  4.73–5.00), as well as acetone ( $\delta$  2.14–2.16) and partially deuterated  $\text{CD}_3\text{OD-d}_4$  ( $\delta$  3.29–3.32) signals) were binned into small segments of equal

widths, providing 174 buckets (i.e., variables) 0.04-ppm wide, with the aid of AMIX software (Analysis of Mixtures software package, Bruker, Karlsruhe, Germany). The areas under each bucket were determined using the special integration mode from AMIX software and then normalized based on the total spectral area and pareto scaling. The buckets (i.e., NMR chemical shifts) were then used as input variables in the chemometric analysis by principal component analysis (PCA), a well-known unsupervised tool for multivariate data exploratory.

#### 4. Conclusions

In this work, metabolite fingerprinting of *Berberis laurina* Billb. (Berberidaceae), a plant well-known for its diversity and pharmacological uses in traditional medicine since ancient times, was achieved for all three sections (leaves, roots, and stems) by means of HR-MAS NMR analysis. HR-MAS NMR-based fingerprinting allowed attaining chemical information directly from samples in their natural, unaltered states, preventing purification steps and preserving the expected status of all fingerprints in the samples and leading to highly reproducible comprehensive results. A total of 17 chemical compounds were identified, including caffeic acid, a recognized compound with plant protective properties, and berberine, a remarked alkaloid of the genus *Berberis* with manifold biological activities. Berberine was found in high amounts in roots, compared to stems and leaves, that, in turn, presented high amounts of caffeic acid (Figure S16). Additionally, a multivariate statistical analysis over HR-MAS NMR spectra from the leaves allowed to realize in a fast and simple way that there is an intrinsic correlation between the changes in the metabolic fingerprint and season time and environmental trend variabilities. All of these findings are supposed to be useful in understanding plant (bio)chemistry, metabolic events, medicinal purposes, health sciences, and genetic and biotechnological research fields.

**Supplementary Materials:** The following are available online, Figure S1: Comparative  $^1\text{H}$  NMR spectra (400 MHz) of plant extract (CD<sub>3</sub>OD solution) and its respective natural state (~10 mg swollen in 40  $\mu\text{L}$  CD<sub>3</sub>OD) from the leaves of *Berberis laurina*, Figure S2: Representative  $^1\text{H}$  HR-MAS NMR spectra acquired directly from different parts of *Berberis laurina* (400 MHz, ~10 mg swollen in 40  $\mu\text{L}$  CD<sub>3</sub>OD), Figure S3:  $^1\text{H}$ - $^{13}\text{C}$  direct correlation map from multiplicity edited HSQC NMR experiment ( $\delta$  6.00–7.65 vs.  $\delta$  110.0–150.0) acquired from leaves of *Berberis laurina* (400 MHz, CD<sub>3</sub>OD). The labels refer to the assignments of intense correlation for compounds as indicate in brackets, Figure S4:  $^1\text{H}$ - $^{13}\text{C}$  direct correlation map from multiplicity edited HSQC NMR experiment ( $\delta$  3.00–5.45 vs.  $\delta$  30.0–140.0) recorded from leaves of *Berberis laurina* (400 MHz, CD<sub>3</sub>OD). The labels refer to the assignments of intense correlation for compounds as indicate in brackets, Figure S5:  $^1\text{H}$ - $^{13}\text{C}$  direct correlation map from multiplicity edited HSQC NMR experiment ( $\delta$  0.60–3.00 vs.  $\delta$  10.0–50.0) recorded from leaves of *Berberis laurina* (400 MHz, CD<sub>3</sub>OD). The labels refer to the assignments of intense correlation for compounds as indicate in brackets, Figure S6:  $^1\text{H}$ - $^{13}\text{C}$  long-range correlation map from HMBC NMR experiment ( $\delta$  0.50–8.00 vs.  $\delta$  5.0–190.0) recorded from leaves of *Berberis laurina* (400 MHz, CD<sub>3</sub>OD). The labels refer to the assignments of intense correlation for compounds as indicate in brackets, Figure S7:  $^1\text{H}$ - $^1\text{H}$  correlation map from COSY NMR experiment ( $\delta$  0.50–8.00 vs.  $\delta$  0.50–8.00) recorded from leaves of *Berberis laurina* (400 MHz, CD<sub>3</sub>OD), Figure S8:  $^1\text{H}$ - $^1\text{H}$  correlation map from TOCSY NMR experiment ( $\delta$  0.50–8.00 vs.  $\delta$  0.50–8.00) recorded from leaves of *Berberis laurina* (400 MHz, CD<sub>3</sub>OD), Figure S9:  $^1\text{H}$ - $^{13}\text{C}$  direct correlation map from multiplicity edited HSQC NMR experiment ( $\delta$  2.96–10.0 vs.  $\delta$  25.0–155.0) recorded from roots of *Berberis laurina* (400 MHz, CD<sub>3</sub>OD). The labels refer to the assignments of intense correlation for compounds as indicate in brackets, Figure S10:  $^1\text{H}$ - $^{13}\text{C}$  long-range correlation map from HMBC NMR experiment ( $\delta$  -1.00–12.00 vs.  $\delta$  -0.5–190.0) recorded from roots of *Berberis laurina* (400 MHz, CD<sub>3</sub>OD), Figure S11:  $^1\text{H}$ - $^1\text{H}$  correlation map from COSY NMR experiment ( $\delta$  -0.50–10.10 vs.  $\delta$  -0.50–10.10) recorded from roots of *Berberis laurina* (400 MHz, CD<sub>3</sub>OD), Figure S12: Climate data from September 2018 to April 2019 in Curitiba, PR, Brazil. Data source: INMET available at <http://www.inmet.gov.br/>, Figure S13: Boxplot regarding signal-to-noise (Y-scale) showing content variability for some compounds over time in the leaves of *Berberis laurina*, Figure S14: Botanical information associated to the species *Berberis laurina* Billb. (Berberidaceae), Figure S15: Schematic representation of applied technology in the current work. This includes a 4-mm HR-MAS rotor containing the sample and its transfer into a NMR spectrometer equipped with and 4-mm HR-MAS probe, in which sample is analyzed under the magic angle direction (54.74°) at moderate spinning speed (5 kHz), Figure S16: A pictorial representation regarding signal-to-noise (S/N) relationships associated to the berberine (15) and caffeic acid (1) contents in leaves (top-bottom), stem, and roots of *Berberis laurina*.

**Author Contributions:** S.A., G.B., A.K. and M.d.F.C.S. were responsible for botanical material collection, NMR measurements and interpretation as well as paper writing. N.N. was responsible for multivariate analysis supervision. A.B., F.R.C. and C.D.R.M.D. were responsible for project conception, general supervision, NMR data supervision and paper writing revision. All authors have read and agreed to the published version of the manuscript

**Funding:** This research was funded in part by TWAS-CNPq grant number 190735/2015-5.

**Acknowledgments:** The authors are incredibly grateful to José Tadeu Weidlich Motta, Marcelo Leandro Brotto, and all staff from the Herbarium of Botanical Garden of Curitiba, Curitiba, PR, Brazil for assistance in plant collection and taxonomic identification. The authors also thank Kelly Mara Seronato (Department of Business Administration, UFPR) for the exceptional assistance.

**Conflicts of Interest:** The authors declare no conflict of interest.

## References

1. Bhardwaj, D.; Kaushik, N. Phytochemical and pharmacological studies in genus *Berberis*. *Phytochem. Rev.* **2012**, *11*, 523–542. [[CrossRef](#)]
2. Landrum, L.R. Revision of *Berberis* (Berberidaceae) in Chile and adjacent southern Argentina. *Ann. Mo. Bot. Gard.* **1999**, *86*, 793. [[CrossRef](#)]
3. Downes, D.P.; Collins, J.H.P.; Lama, B.; Zeng, H.; Nguyen, T.; Keller, G.; Febo, M.; Long, J. Characterization of brain metabolism by nuclear magnetic resonance. *ChemPhysChem* **2018**, *20*, 216–230. [[CrossRef](#)] [[PubMed](#)]
4. Hatzakis, E. Nuclear Magnetic Resonance (NMR) spectroscopy in food science: A comprehensive review. *Compr. Rev. Food Sci. Food Saf.* **2019**, *18*, 189–220. [[CrossRef](#)]
5. Kaneko, G.; Ushio, H.; Ji, H. Application of magnetic resonance technologies in aquatic biology and seafood science. *Fish. Sci.* **2019**, *85*, 1–17.
6. Kumar, A.; Kuhn, L.T.; Balbach, J. In-cell NMR: Analysis of protein–small molecule interactions, metabolic processes, and protein phosphorylation. *Int. J. Mol. Sci.* **2019**, *20*, 378. [[CrossRef](#)] [[PubMed](#)]
7. Nikitin, K.; O’Gara, R. Mechanisms and beyond: Elucidation of fluxional dynamics by exchange NMR spectroscopy. *Chem. Eur. J.* **2019**, *25*, 4551–4589. [[CrossRef](#)]
8. Pautler, B.G.; Simpson, A.J.; Simpson, M.J.; Tseng, L.-H.; Spraul, M.; Dubnick, A.; Sharp, M.J.; Fitzsimons, S.J. Detection and structural identification of dissolved organic matter in antarctic glacial ice at natural abundance by SPR-W5-WATERGATE <sup>1</sup>H NMR spectroscopy. *Environ. Sci. Technol.* **2011**, *45*, 4710–4717. [[CrossRef](#)] [[PubMed](#)]
9. Rudsuck, T.; Förster, E.; Nirschl, H.; Guthausen, G. Low-field NMR for quality control on oils. *Magn. Reson. Chem.* **2019**, *57*, 777–793. [[CrossRef](#)] [[PubMed](#)]
10. Vignoli, A.; Ghini, V.; Meoni, G.; Licari, C.; Takis, P.G.; Tenori, L.; Turano, P.; Luchinat, C. High-throughput metabolomics by 1D NMR. *Angew. Chem. Int. Ed.* **2019**, *58*, 968–994. [[CrossRef](#)]
11. Lee, K.-M.; Jeon, J.-Y.; Lee, B.-J.; Lee, H.; Choi, H.-K. Application of metabolomics to quality control of natural product derived medicines. *Biomol. Ther.* **2017**, *25*, 559–568. [[CrossRef](#)] [[PubMed](#)]
12. Simmler, C.; Graham, J.G.; Chen, S.-N.; Pauli, G.F. Integrated analytical assets aid botanical authenticity and adulteration management. *Fitoterapia* **2018**, *129*, 401–414.
13. Yun, D.-Y.; Kang, Y.-G.; Kim, E.-H.; Kim, M.; Park, N.-H.; Choi, H.-T.; Go, G.H.; Lee, J.H.; Park, J.S.; Hong, Y.-S. Metabolomics approach for understanding geographical dependence of soybean leaf metabolome. *Food Res. Int.* **2018**, *106*, 842–852. [[CrossRef](#)] [[PubMed](#)]
14. Kuballa, T.; Brunner, T.S.; Thongpanchang, T.; Walch, S.G.; Lachenmeier, D.W. Application of NMR for authentication of honey, beer and spices. *Curr. Opin. Food Sci.* **2018**, *19*, 57–62. [[CrossRef](#)]
15. Zhang, Y.; Wu, H.; Wei, L.; Xie, Z.; Guan, B. Effects of hypoxia in the gills of the Manila clam *Ruditapes philippinarum* using NMR-based metabolomics. *Mar. Pollut. Bull.* **2017**, *114*, 84–89. [[CrossRef](#)]
16. Zanatta, M.; Simon, N.M.; dos Santos, F.P.; Corvo, M.C.; Cabrita, E.J.; Dupont, J. Correspondence on “preorganization and cooperation for highly efficient and reversible capture of low-concentration CO<sub>2</sub> by ionic liquids”. *Angew. Chem. Int. Ed.* **2019**, *58*, 382–385. [[CrossRef](#)]
17. Lam, B.; Simpson, A.J. Direct <sup>1</sup>H NMR spectroscopy of dissolved organic matter in natural waters. *Analyst* **2008**. [[CrossRef](#)] [[PubMed](#)]
18. Wong, A.; Lucas-Torres, C. High-resolution magic-angle spinning (HR-MAS) NMR spectroscopy. In *NMR-Based Metabolomics*; Keun, H.C., Ed.; The Royal Society of Chemistry: London, UK, 2018; pp. 133–150.
19. Flores, I.S.; Martinelli, B.C.B.; Pinto, V.S.; Queiroz, L.H.K.; Lião, L.M. Important issues in plant tissues analyses by HR-MAS NMR. *Phytochem. Anal.* **2019**, *30*, 5–13. [[CrossRef](#)] [[PubMed](#)]
20. Jensen, H.M.; Bertram, H.C. The magic angle view to food: Magic-angle spinning (MAS) NMR spectroscopy in food science. *Metabolomics* **2019**, *15*, 44. [[CrossRef](#)] [[PubMed](#)]

21. Alam, T.M.; Jenkins, J.E. HR-MAS NMR spectroscopy in material science. In *Advanced Aspects of Spectroscopy*; Farrukh, M.A., Ed.; IntechOpen: London, UK, 2012; pp. 279–306.
22. Farooq, H.; Courtier-Murias, D.; Soong, R.; Bermel, W.; Kingery, W.; Simpson, A. HR-MAS NMR spectroscopy: A practical guide for natural samples. *Curr. Org. Chem.* **2013**, *17*, 3013–3031. [[CrossRef](#)]
23. Mazzei, P.; Piccolo, A.; Valentini, M. Intact food analysis by means of HRMAS-NMR spectroscopy. In *Modern Magnetic Resonance*; Springer International Publishing: Cham, Switzerland, 2018; pp. 1503–1518.
24. Gribbestad, I.S.; Aursand, M.; Martinez, I. High-resolution  $^1\text{H}$  magnetic resonance spectroscopy of whole fish, fillets and extracts of farmed Atlantic salmon (*Salmo salar*) for quality assessment and compositional analyses. *Aquaculture* **2005**, *250*, 445–457. [[CrossRef](#)]
25. Igarashi, T.; Aursand, M.; Hirata, Y.; Gribbestad, I.S.; Wada, S.; Nonaka, M. Nondestructive quantitative determination of docosahexaenoic acid and n–3 fatty acids in fish oils by high-resolution  $^1\text{H}$  nuclear magnetic resonance spectroscopy. *J. Am. Oil Chem. Soc.* **2000**, *77*, 737–748. [[CrossRef](#)]
26. García-García, A.B.; Lamichhane, S.; Castejón, D.; Cambero, M.I.; Bertram, H.C.  $^1\text{H}$  HR-MAS NMR-based metabolomics analysis for dry-fermented sausage characterization. *Food Chem.* **2018**, *240*, 514–523. [[CrossRef](#)] [[PubMed](#)]
27. Prabhu, V.V.; Nguyen, T.B.; Cui, Y.; Oh, Y.-E.; Piao, Y.-H.; Baek, H.-M.; Kim, J.J.-Y.; Shin, K.-H.; Kim, J.J.-Y.; Lee, K.-H.; et al. Metabolite signature associated with stress susceptibility in socially defeated mice. *Brain Res.* **2019**, *1708*, 171–180. [[CrossRef](#)] [[PubMed](#)]
28. Hassan, Q.; Dutta Majumdar, R.; Wu, B.; Lane, D.; Tabatabaei-Anraki, M.; Soong, R.; Simpson, M.J.; Simpson, A.J. Improvements in lipid suppression for  $^1\text{H}$  NMR-based metabolomics: Applications to solution-state and HR-MAS NMR in natural and in vivo samples. *Magn. Reson. Chem.* **2019**, *57*, 69–81. [[CrossRef](#)] [[PubMed](#)]
29. Ocampos, F.M.M.; Menezes, L.R.A.; Dutra, L.M.; Santos, M.F.C.; Ali, S.; Barison, A. NMR in chemical ecology: An overview highlighting the main NMR approaches. In *eMagRes*; John Wiley & Sons, Ltd.: Chichester, UK, 2017; Volume 6, pp. 325–342.
30. Santos, A.D.C.; Fonseca, F.A.; Lião, L.M.; Alcantara, G.B.; Barison, A. High-resolution magic angle spinning nuclear magnetic resonance in foodstuff analysis. *Trends Anal. Chem.* **2015**, *73*, 10–18. [[CrossRef](#)]
31. Dumez, J.-N. Spatial encoding and spatial selection methods in high-resolution NMR spectroscopy. *Prog. Nucl. Magn. Reson. Spectrosc.* **2018**, *109*, 101–134. [[CrossRef](#)] [[PubMed](#)]
32. Sampaio, B.L.; Edrada-Ebel, R.; da Costa, F.B. Effect of the environment on the secondary metabolic profile of *Tithonia diversifolia*: A model for environmental metabolomics of plants. *Sci. Rep.* **2016**, *6*, 29265. [[CrossRef](#)]
33. Van Rensburg, H.C.J.; van den Ende, W.; Signorelli, S. Autophagy in plants: Both a puppet and a puppet master of sugars. *Front. Plant Sci.* **2019**, *10*, 10. [[CrossRef](#)]
34. Shahbazy, M.; Moradi, P.; Ertaylan, G.; Zahraei, A.; Kompany-Zareh, M. FTICR mass spectrometry-based multivariate analysis to explore distinctive metabolites and metabolic pathways: A comprehensive bioanalytical strategy toward time-course metabolic profiling of *Thymus vulgaris* plants responding to drought stress. *Plant Sci.* **2020**, *290*, 110257. [[CrossRef](#)]
35. Fait, A.; Batushansky, A.; Shrestha, V.; Yobi, A.; Angelovici, R. Can metabolic tightening and expansion of co-expression network play a role in stress response and tolerance? *Plant Sci.* **2020**, *293*, 110409. [[CrossRef](#)] [[PubMed](#)]
36. Sari, Z.K.A. Phytochemical investigations on chemical constituents of taraxacum bessarabicum (Hornem.) hand.-mazz. subsp. bessarabicum (Hornem.) hand.-mazz. *Iran. J. Pharm. Res.* **2019**, *18*, 400–405. [[PubMed](#)]
37. Liu, Q.; Luo, L.; Zheng, L. Lignins: Biosynthesis and biological functions in plants. *Int. J. Mol. Sci.* **2018**, *19*, 335. [[CrossRef](#)] [[PubMed](#)]
38. Boerjan, W.; Ralph, J.; Baucher, M. Lignin biosynthesis. *Annu. Rev. Plant Biol.* **2003**, *54*, 519–546. [[CrossRef](#)]
39. Chander, V.; Aswal, J.S.; Dobhal, R.; Uniyal, D.P. A review on pharmacological potential of berberine; an active component of himalayan berberis aristata. *J. Phytopharm.* **2017**, *6*, 53–58.
40. Bhatia, A.; Tripathi, T.; Singh, S.; Bisht, H.; Behl, H.M.; Roy, R.; Sidhu, O.P. Comprehensive metabolite profiling in distinct chemotypes of *Commiphora wightii*. *Nat. Prod. Res.* **2019**, *33*, 17–23. [[CrossRef](#)]
41. Chia, D.W.; Yoder, T.J.; Reiter, W.D.; Gibson, S.I. Fumaric acid: An overlooked form of fixed carbon in Arabidopsis and other plant species. *Planta* **2000**, *211*, 743–751. [[CrossRef](#)] [[PubMed](#)]
42. Shakya, A.; Singh, G.; Chatterjee, S.; Kumar, V. Role of fumaric acid in anti-inflammatory and analgesic activities of a *Fumaria indica* extracts. *J. Intercult. Ethnopharmacol.* **2014**, *3*, 173–178. [[CrossRef](#)]

43. Papadopoulos, K.; Triantis, T.; Dimotikali, D.; Nikokavouras, J. Evaluation of food antioxidant activity by photostorage chemiluminescence. *Anal. Chim. Acta* **2001**, *433*, 263–268. [[CrossRef](#)]
44. Leyva-Peralta, M.A.; Robles-Zepeda, R.E.; Garibay-Escobar, A.; Ruiz-Bustos, E.; Alvarez-Berber, L.P.; Gálvez-Ruiz, J.C. In vitro anti-proliferative activity of Argemone gracilentia and identification of some active components. *BMC Complement. Altern. Med.* **2015**, *15*, 13. [[CrossRef](#)] [[PubMed](#)]
45. Srivastava, S.; Srivastava, M.; Misra, A.; Pandey, G.; Rawat, A. A review on biological and chemical diversity in Berberis (Berberidaceae). *EXCLI J.* **2015**, *14*, 247–267.
46. Tsujimoto, T.; Yoshitomi, T.; Maruyama, T.; Yamamoto, Y.; Hakamatsuka, T.; Uchiyama, N. <sup>13</sup>C-NMR-based metabolic fingerprinting of Citrus-type crude drugs. *J. Pharm. Biomed. Anal.* **2018**, *161*, 305–312. [[CrossRef](#)]
47. Gil, A.M.; Duarte, I.F.; Delgadillo, I.; Colquhoun, I.J.; Casuscelli, F.; Humpfer, E.; Spraul, M. Study of the compositional changes of mango during ripening by use of nuclear magnetic resonance spectroscopy. *J. Agric. Food Chem.* **2000**, *48*, 1524–1536. [[CrossRef](#)]
48. Muthuramalingam, P.; Krishnan, S.R.; Pandian, S.; Mareeswaran, N.; Aruni, W.; Pandian, S.K.; Ramesh, M. Global analysis of threonine metabolism genes unravel key players in rice to improve the abiotic stress tolerance. *Sci. Rep.* **2018**, *8*, 9270. [[CrossRef](#)] [[PubMed](#)]
49. Lenka, S.K.; Katiyar, A.; Chinnusamy, V.; Bansal, K.C. Comparative analysis of drought-responsive transcriptome in Indica rice genotypes with contrasting drought tolerance. *Plant Biotechnol. J.* **2011**, *9*, 315–327. [[CrossRef](#)] [[PubMed](#)]
50. Barison, A.; da Silva, C.W.P.; Campos, F.R.R.; Simonelli, F.; Lenz, C.A.A.; Ferreira, A.G. A simple methodology for the determination of fatty acid composition in edible oils through <sup>1</sup>H NMR spectroscopy. *Magn. Reson. Chem.* **2010**, *48*, 642–650. [[CrossRef](#)] [[PubMed](#)]
51. Ali, K.; Maltese, F.; Zyprian, E.; Rex, M.; Choi, Y.H.; Verpoorte, R. NMR metabolic fingerprinting based identification of grapevine metabolites associated with downy mildew resistance. *J. Agric. Food Chem.* **2009**, *57*, 9599–9606. [[CrossRef](#)]
52. Kim, H.K.; Choi, Y.H.; Verpoorte, R. NMR-based metabolomic analysis of plants. *Nat. Protoc.* **2010**, *5*, 536–549. [[PubMed](#)]
53. Azmat, R.; Haider, S.; Nasreen, H.; Aziz, F.; Riaz, M. A viable alternative mechanism in adapting the plants to heavy metal environment. *Pakistan J. Bot.* **2009**, *41*, 2729–2738.
54. Iqbal, M.; Mushta, M.Y.; Ali, K.; Korthout, H.A.A.J.; Verpoorte, R.; Cardozo, M.L.; Ordoñez, R.M.; Isla, M.I.; Choi, Y.H. NMR Spectroscopy Coupled with Multivariate Data Analysis to Assess Antiinflammatory Activities of Eugenia Uniflora Fruits in Different Developmental Stages. Ph.D. Thesis, Leiden University, Leiden, The Netherlands, 2013.
55. Ravaglia, L.M.; Pizzotti, A.B.C.; Alcantara, G.B. NMR-based and chemometric approaches applicable to adulteration studies for assessment of the botanical origin of edible oils. *J. Food Sci. Technol.* **2019**, *56*, 507–511. [[CrossRef](#)] [[PubMed](#)]
56. Neag, M.A.; Mocan, A.; Echeverría, J.; Pop, R.M.; Bocsan, C.I.; Crişan, G.; Buzoianu, A.D.; Crisan, G.; Buzoianu, A.D.; Crişan, G. Berberine: Botanical occurrence, traditional uses, extraction methods, and relevance in cardiovascular, metabolic, hepatic, and renal disorders. *Front. Pharmacol.* **2018**, *9*. [[CrossRef](#)] [[PubMed](#)]
57. Kumar, R.; Bohra, A.; Pandey, A.K.; Pandey, M.K.; Kumar, A. Metabolomics for plant improvement: Status and prospects. *Front. Plant Sci.* **2017**, *8*. [[CrossRef](#)] [[PubMed](#)]
58. Pavarini, D.P.; Pavarini, S.P.; Niehues, M.; Lopes, N.P. Exogenous influences on plant secondary metabolite levels. *Anim. Feed Sci. Technol.* **2012**, *176*, 5–16. [[CrossRef](#)]
59. Yang, L.; Wen, K.S.; Ruan, X.; Zhao, Y.X.; Wei, F.; Wang, Q. Response of plant secondary metabolites to environmental factors. *Molecules* **2018**, *23*, 762. [[CrossRef](#)] [[PubMed](#)]
60. Ncube, B.; Finnie, J.F.; Van Staden, J. Quality from the field: The impact of environmental factors as quality determinants in medicinal plants. *S. Afr. J. Bot.* **2012**, *82*, 11–20. [[CrossRef](#)]
61. Jahangir, M.; Nuringtyas, T.R.; Ali, K.; Wilson, E.G.; Choi, Y.H.; Verpoorte, R. NMR-based metabolomics: Understanding plant chemistry and identification of biologically active compounds. In *NMR-Based Metabolomics*; Keun, H.C., Ed.; The Royal Society of Chemistry: London, UK, 2018; pp. 246–263.
62. Emwas, A.-H.; Saccenti, E.; Gao, X.; McKay, R.T.; dos Santos, V.A.P.M.; Roy, R.; Wishart, D.S. Recommended strategies for spectral processing and post-processing of 1D <sup>1</sup>H-NMR data of biofluids with a particular focus on urine. *Metabolomics* **2018**, *14*, 31. [[CrossRef](#)] [[PubMed](#)]

63. Ebrahimi, P.; Viereck, N.; Bro, R.; Engelsen, S.B. Chemometric analysis of NMR spectra. In *Modern Magnetic Resonance*; Springer International Publishing: Cham, Germany, 2018; pp. 1649–1668, ISBN 9783319283883.
64. Engel, J.; Gerretzen, J.; Szymańska, E.; Jansen, J.J.; Downey, G.; Blanchet, L.; Buydens, L.M.C. Breaking with trends in pre-processing? *Trends Anal. Chem.* **2013**, *50*, 96–106. [[CrossRef](#)]

**Sample Availability:** Samples of the compounds were identified directly on the botanical material.



© 2020 by the authors. Licensee MDPI, Basel, Switzerland. This article is an open access article distributed under the terms and conditions of the Creative Commons Attribution (CC BY) license (<http://creativecommons.org/licenses/by/4.0/>).